NACA

RESEARCH MEMORANDUM

GENERAL THEORY OF WAVE-DRAG REDUCTION FOR COMBINATIONS EMPLOYING QUASI-CYLINDRICAL BODIES WITH AN APPLICATION TO SWEPT-WING AND BODY COMBINATIONS

By Jack N. Nielsen

Ames Aeronautical Laboratory
Moffett Field, Calif.

NATIONAL ADVISORY COMMITTEE
FOR AERONAUTICS

WASHINGTON

June 24, 1955

TABLE OF CONTENTS

NATIONAL ADVISORY COMMITTEE FOR AERONAUTICS

RESEARCH MEMORANDUM

GENERAL THEORY OF WAVE-DRAG REDUCTION FOR COMBINATIONS EMPLOYING QUASI-CYLINDRICAL BODIES WITH AN APPLICATION TO SWEPT-WING AND BODY COMBINATIONS

By Jack N. Nielsen

SUMMARY

The wing-body interference theory of NACA TN 2677 applied to symmetrical wings in combination with quasi-cylindrical bodies permits the direct calculation of pressure-distribution changes produced by body shape changes. This theory is used to determine the relative magnitude of the wave-drag reduction produced by changes in cylinder cross-sectional area and that produced by changes in cross-sectional shape (without change in area). The body distortion is expressed as a Fourier series, and an integral equation is derived for the body shape for minimum drag for each Fourier component. Thus the wave-drag reductions for the various Fourier harmonics are independent and additive.

To demonstrate the use of the method, it is applied to a body with a 45° swept wing having a chord of three body radii, a span of six body radii, sonic leading and trailing edges, and a biconvex airfoil section. The axially symmetric harmonic of body distortion caused a reduction of wave drag of 22 percent of the drag of the wing panels on the cylindrical undistorted body. However, the second harmonic, which causes no change in volume, produced a drag saving of 42 percent. The wave-drag saving was obtained by decreasing the wing-panel drag by twice as much as the body drag was increased. The wing panels have negative wave drag for two harmonics. These reductions are accompanied by pressure gradients that are adverse for the boundary layer. With regard to fuselage shape, volume is removed from the sides of the fuselage and added to the top and bottom. A net volume less than the wing volume is removed if the distortions are limited to the interval of the root chord. Although the second harmonic removes no volume, it causes indentations about five times as deep as those due to the axially symmetric harmonic. As a result the wing thickness for which the full theoretical distortions can be utilized is limited to about 5 percent.

A very simple theory for the axially symmetric harmonic can be derived by neglecting three-dimensional effects. This theory is valid

for small chord lengths. However, an approximate treatment of the three-dimensional effects yields a fairly simple theory applicable to longer chord lengths. The effects of semispan-radius ratio and chord-radius ratio on indentation shape, indentation volume, and drag saving have been determined using the approximate theories for the axially symmetric harmonic.

INTRODUCTION

The experimental verification by Whitcomb (ref. 1) of the area rule has opened up a new realm of possibilities of reducing the wave drag of complete configurations at transonic and supersonic speeds. The theoretical basis for the area rule lay undiscovered for some time in the Hayes drag formula (ref. 2), which contains the implication that by indenting a body, a saving in wave drag equal to the drag of the wing panels can be produced. Thus, in principle, the wave drag of a slender combination utilizing an infinite cylindrical body can be reduced to zero. More recently Lomax and Heaslet (ref. 3) have proposed the following method for determining wing-body combinations of minimum wave drag. Starting initially with a wing alone, they

(1) use the invariance principle of Hayes to find distributions of multipoles along the longitudinal axis that represent the wing-alone flow field at large radial distances

(2) designate the negatives of the multipole distributions as canceling multipoles, place them along the longitudinal axis, and calculate a stream tube in the vicinity of the wing.

The wing-body combination given by (2) has zero wave drag if all multipoles are used. If, to obtain practical shapes, only a finite number of multipoles are used, the wave drag is a minimum for this number.

In the foregoing method the problems of actual body shape and of pressure distributions are secondary considerations in the mathematical solution of the minimum-wave-drag problem. A method for minimizing wave drag of wing-body combinations dealing directly with the body shape and the pressure distributions has been developed based on the interference theory of references 4, 5, and 6. The method, presented herein, is applicable to combinations with bodies which are approximately cylindrical in the region of the wing. There are no restrictions on the Mach number as long as it is greater than unity but not hypersonic. The principal restriction on the wing other than small thickness and sharp leading edges is that it possess a horizontal plane of symmetry or that its upper and lower surfaces be independent. It is the purpose of this paper to present in the first part a general theory of drag reduction for wings on quasi-cylindrical bodies. In the second part the method is

applied to the reduction in wave drag of a combination employing a swept wing with sonic edges.

SYMBOLS

All lengths are measured in body radii.

a	body radius
A_E	aspect ratio of exposed wing panels joined together
c	local wing chord or chord of rectangular wing
c_r	chord at wing-body juncture
C_D	wave-drag coefficient of combination based on exposed wing area
C_{D_S}	reduction in drag coefficient based on exposed wing area as a result of body distortion
$D_{B(C)}$	drag of body in combination
$D_{B(C)_{2n}}$	drag of body due to 2nth Fourier harmonic
D_C	drag of combination
D_S	saving in drag of combination by body distortion
$D_{W(d)}$	drag of wing in combination with body due to body distortion
$D_{W(i)}$	drag of wing in combination with body due to interference
$D_{W(i+d)}^{(1)}$	drag of wing in combination due to interference and distortion pressures propagated along characteristic body cones
$D_{W(i+d)}^{(2)}$	drag of wing in combination due to interference and distortion pressures falling behind characteristic body cones
$D_{W(C)}$	drag of wing panels on distorted body
$D_{W(W)}$	drag of wing panels acting as part of wing alone
$\frac{dz}{dx}$	local slope of wing surface in streamwise direction

[redacted]

$f_{2n}(x)$ velocity amplitude function of 2nth harmonic neglecting tip effects

$f_{2n_s}(x)$ velocity amplitude function for a pair of opposing sources inclined at the Mach angle

$g_{2n}(x)$ amplitude of body distortion due to 2nth harmonic

$g_o^{(1)}$, $g_o^{(2)}$, . . . successive approximations to $g_o(x)$

$h_{2n}(x)$ nonhomogeneous part of integral equation for $g_{2n}(x)$

$h_{o_1}(x)$, $h_{o_2}(x)$, $h_{o_3}(x)$, components of $h_o(x)$

l upstream limit of body distortion

m slope of wing leading edge

M free-stream Mach number

n normal to quasi-cylindrical body

$2n$ index of Fourier harmonics

p local static pressure

$p_{2n}(x)$ half-amplitude of the 2nth Fourier component of the pressure acting on the body due to the wing alone neglecting tip effects

p_∞ free-stream static pressure

P pressure coefficient, $\frac{p - p_\infty}{q}$

$P_{B(d)}$ body pressure coefficient due to body distortions

$P_{B(i)}$ body pressure coefficient due to interference

$P_{B(W)}$ body pressure coefficient due to wing alone

$P_{W(d)}$ wing pressure coefficient due to body distortions

$P_{W(i)}$	wing pressure coefficient due to interference
$P_{W(W)}$	wing pressure coefficient due to wing alone
q	free-stream dynamic pressure, $\frac{1}{2}\rho V^2$
r,θ	polar coordinates in y,z plane; $y = r \cos \theta$, $z = r \sin \theta$
r_B	radial distance to point on body of combination
R.P.	real part of a complex function
s	semispan of wing-body combination
$s_i(x)$	local semispan of inner portion of wing plan form (sketch (c))
$s_o(x)$	local semispan of outer portion of wing plan form (sketch (c))
S_P	area of one exposed wing panel
S_W	area of two exposed wing panels
t_m	maximum thickness of wing section
u,v,w	perturbation velocities along x, y, and z axes, respectively
v_n	velocity normal to quasi-cylindrical body, positive outward
v_r	velocity along radius vector, positive outward
V	free-stream velocity
V_i	volume of body indentation
V_W	volume of exposed wing
$W_{2n}(x,r)$	influence function
x,y,z	coordinate axes with origin at vertex of wing alone, x measured downstream, y laterally to the pilot's right, and z vertically upward
x_1	intersection with body of most forward body characteristic touching exposed wing
x_2	intersection with body of most rearward body characteristic touching exposed wing

x',y',z' oblique coordinates; $x' = x - my$, $y' = y - mx$, $z' = z\sqrt{1 - m^2}$

$Y(x)$ $\int_0^x W_0(\xi)d\xi$

$Z(x)$ $\int_0^x \xi W_0(\xi)d\xi$

z_l local thickness of lower wing surface measured from chord plane, $z = 0$

z_u local thickness of upper wing surface measured from chord plane, $z = 0$

β $\sqrt{M^2 - 1}$

$\Gamma_{2n}(x,s)$ $\int_1^s W_{2n}(x,r)dr$

ϵ semiapex angle of wing section

η function defining the plan-form distribution of wing thickness (eq. (2))

λ_n constant, $\lambda_0 = 4$, $\lambda_n = 2$ if $n > 0$

ρ free-stream density

φ_B potential of distorted body alone

φ_C potential of complete combination

φ_i interference potential, $\varphi_C - (\varphi_W + \varphi_B)$

φ_W potential of wing alone

An asterisk (*) distinguishes a quantity associated with the wing tip.

I - GENERAL THEORY

Statement of Problem and Determination of Boundary Conditions

In references 4, 5, and 6 the boundary-value problem of determining the pressure distribution acting on a combination composed of a wing and

an infinite, circular, cylindrical body was solved. In the method, the flow field of the wing alone is pictured as causing a virtual distortion of the body surface, and the pressure field due to such distortion is computed term by term for each Fourier harmonic of the distortion. The pressure field on the body is computed with the help of a table of characteristic functions or influence coefficients which give the pressure coefficient at any point of the body due to a unit bump at the origin. By summing the pressure contributions of each bump on the body by numerical integration, the entire pressure field is built up. An essentially different and more complicated method using axial distributions of sources and multipoles was used to obtain the pressure field off the body. However, it has recently been possible to extend the method for computing the pressures for points on the body to points off the body by expanding the tables of influence coefficients. The theory of the new method is set forth in Appendix A. This method which has been applied to combinations with cylindrical bodies having virtual distortions is equally applicable to combinations having bodies with real distortions. Thus we can evaluate the pressure field and the pressure drag of a combination with a body of arbitrary small distortion using the above methods. The pressure drag of the combination can be minimized with respect to body shape by the calculus of variations to determine the best shape for minimum drag. In this part of the report the theory of determining this shape will be considered.

In this paper the wing alone is taken to be the wing panels plus the portion of the wing blanketed by the body when the leading- and trailing-edge intersections with the body are joined across the body in any arbitrary manner. The wing-body combinations to which the analysis applies possess a vertical plane of symmetry and either a horizontal plane of symmetry or upper and lower wing surfaces that are independent (e.g., a triangular wing with supersonic leading edges). An additional assumption is that the body shape at any point does not greatly deviate from a circular cylinder; that is, the body is quasi-cylindrical. Sketch (a) illustrates the winged portion of a wing-body combination together with the system of axes used in the analysis. All distances are based on a radius of unity so that the formulas in the analysis can be written in simple form. The body cross section at any x position is taken as a circle on which are superimposed distortions that vary as cosines of even multiples of θ to preserve a vertical plane of symmetry. Thus

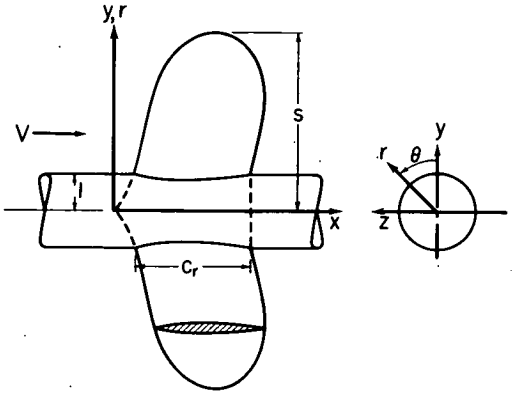

Sketch (a)

$$\left.\frac{\partial r}{\partial x}\right]_{r=1} = \left(\frac{t_m}{c_r}\right)\sum_{n=0}^{\infty} g_{2n}(x)\cos 2n\theta \qquad (1)$$

[redacted]

The function $g_{2n}(x)$ is the shape amplitude function of the 2nth Fourier harmonic and is to be so determined that the wave drag is a minimum. With regard to the wing, no limitations are made on its plan form. The coordinates of the wing section at any spanwise station y are taken to be

$$z_u = -z_l = t_m \eta(x - \beta r + \beta, r) \tag{2}$$

where η is a function giving the thickness distribution and is zero off the wing.

Consider now the boundary-value problem of determining the combination potential. This problem is solved in essentially the same manner as in reference 4. For a cylindrical body the combination potential is the sum of the wing-alone and interference potentials, but when the body is distorted, an extra potential φ_B must be added.

$$\varphi_C = \varphi_W + \varphi_i + \varphi_B \tag{3}$$

All potentials are to satisfy the wave equation in cylindrical coordinates.

$$\frac{\partial^2 \varphi}{\partial r^2} + \frac{1}{r}\frac{\partial \varphi}{\partial r} + \frac{1}{r^2}\frac{\partial^2 \varphi}{\partial \theta^2} - \frac{\partial^2 \varphi}{\partial x^2} = 0$$

The first boundary condition is that the derivative of the combination potential normal to both wing and body be zero with the body taken as the $r = 1$ cylinder and the wing as the $z = 0$ plane. Thus

$$\frac{\partial \varphi_C}{\partial n} = 0 \qquad \begin{array}{lll} r = 1 & 0 \le \theta \le 2\pi & \text{(body)} \\ r \ge 1 & \theta = 0, \pi & \text{(wing)} \end{array} \tag{4a}$$

The second boundary condition is that there be no upstream waves.

$$\varphi_C = 0 \qquad x \le 0 \tag{4b}$$

The second boundary condition is satisfied naturally by using Laplace transform methods, but the first one is not so easily met. Consider

[redacted]

sketch (b) which shows a region of the quasi-cylindrical surface $R(x,r,\theta)$ = constant in the neighborhood of point P. The direction cosines of the normal to the surface at point P are

$$\frac{\partial R/\partial x}{|\text{grad } R|}, \frac{\partial R/\partial r}{|\text{grad } R|}, \frac{1}{r}\frac{\partial R/\partial \theta}{|\text{grad } R|}$$

The velocity in the normal direction is thus

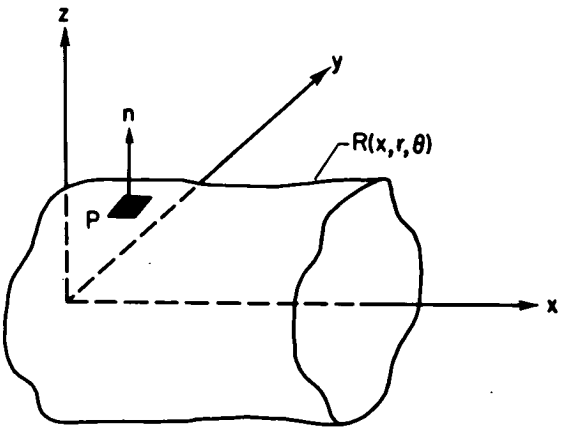

Sketch (b)

$$v_n = \frac{\partial R/\partial x}{|\text{grad } R|}\frac{\partial \varphi_C}{\partial x} + \frac{\partial R/\partial r}{|\text{grad } R|}\frac{\partial \varphi_C}{\partial r} + \frac{\partial R/\partial \theta}{r^2|\text{grad } R|}\frac{\partial \varphi_C}{\partial \theta} = 0$$

For a quasi-cylindrical body the equation of the body surface is

$$R(x,r,\theta) = r - \left(\frac{t_m}{c_r}\right)\sum_{n=o}^{\infty}\cos 2n\theta \int_o^x g_{2n}(\xi)d\xi = 1$$

so that

$$\frac{\partial R}{\partial x} = 0\left(\frac{t_m}{c_r}\right), \frac{\partial R}{\partial r} = 1, \frac{\partial R}{\partial \theta} = 0\left(\frac{t_m}{c_r}\right)$$

Since

$$\frac{\partial \varphi_C}{\partial x} \approx V, \frac{\partial \varphi_C}{\partial r} = 0\left(\frac{t_m}{c_r}\right), \frac{\partial \varphi_C}{\partial \theta} = 0\left(\frac{t_m}{c_r}\right)$$

the third term in the equation for v_n is negligible compared to the first two terms so that

$$\frac{\partial \varphi_C}{\partial r} \approx -\frac{\partial \varphi_C}{\partial x}\frac{\partial R}{\partial x} \approx -V\frac{\partial R}{\partial x}; \qquad r = 1 \tag{5}$$

Combining equations (1) and (5) yields the boundary condition for zero normal velocity at the body surface

$$\frac{\partial \varphi_C}{\partial r} = \frac{\partial \varphi_W}{\partial r} + \frac{\partial \varphi_i}{\partial r} + \frac{\partial \varphi_B}{\partial r} = V\left(\frac{t_m}{c_r}\right) \sum_{n=0}^{\infty} g_{2n}(x)\cos 2n\theta; \qquad r = 1,\ 0 \leq \theta \leq 2\pi \tag{6}$$

For no flow normal to the wing surface, we obtain

$$\frac{\partial \varphi_C / \partial z}{V} = \frac{\partial z_u}{\partial x}$$

In terms of potential functions this boundary condition becomes

$$\frac{\partial \varphi_C}{\partial z} = \frac{1}{r}\frac{\partial \varphi_C}{\partial \theta} = \frac{1}{r}\left(\frac{\partial \varphi_W}{\partial \theta} + \frac{\partial \varphi_i}{\partial \theta} + \frac{\partial \varphi_B}{\partial \theta}\right) = V\frac{\partial z_u}{\partial x}; \qquad r \geq 1;\ \theta = 0, \pi \tag{7}$$

Equation (7) is fulfilled by expanding φ_i and φ_B in cosine series of even multiples of θ. Equation (6) is fulfilled by satisfying the following equations for each term of the Fourier series as in reference 4.

$$\frac{\partial \varphi_i}{\partial r} = -\frac{\partial \varphi_W}{\partial r} = V\left(\frac{t_m}{c_r}\right) \sum_{n=0}^{\infty} f_{2n}(x)\cos 2n\theta$$

$$\frac{\partial \varphi_B}{\partial r} = V\left(\frac{t_m}{c_r}\right) \sum_{n=0}^{\infty} g_{2n}(x)\cos 2n\theta$$

It is to be remembered that φ_i is the interference potential defined so that the combination possesses a cylindrical fuselage. It changes if the definition of the wing alone changes. All effects of distorting the circular cylinder are contained in φ_B.

Pressure Field Acting on Wing-Body Combination

The first step in the present method for evaluating the drag of a wing-body combination is to determine the pressure distribution acting

[redacted]

on the combination. This can be done for the body very simply by means of the $W_{2n}(x)$ functions tabulated in reference 5. The pressure field off the body has been obtained in references 4 and 5 by distributing multipoles along the body axis. However, the determination of the pressure field off the body can be reduced to the same amount of work as determining that on the body by generalizing the $W_{2n}(x)$ functions to $W_{2n}(x,r)$ functions. This new procedure besides vastly simplifying the calculation of the pressures off the body also avoids the necessity of integrating across logarithmic singularities involved in the original method. The generalization of the $W_{2n}(x)$ functions to $W_{2n}(x,r)$ functions and their use in calculating the pressure field off the body are described in Appendix A. The $W_{2n}(x,r)$ functions are plotted for $n = 0$ and 1 in figure 1.

The pressure coefficients of the combination are the sums of the coefficients due to the body alone, wing alone, and interference. According to Appendix A the pressure field due to the body alone (distorted) is given on the body and the wing as

$$\frac{P_{B(d)}}{(t_m/c_r)} = \frac{2}{\beta} \sum_{n=0}^{\infty} \left[g_{2n}(x) - \frac{1}{\beta} \int_0^x g_{2n}(\xi) W_{2n}\left(\frac{x-\xi}{\beta}, 1 \right) d\xi \right] \cos 2n\theta \qquad (8)$$

$$\frac{P_{W(d)}}{(t_m/c_r)} = \frac{2}{\beta} \sum_{n=0}^{\infty} \left[\frac{g_{2n}(x - \beta r + \beta)}{\sqrt{r}} - \frac{1}{\beta} \int_0^{x-\beta(r-1)} g_{2n}(\xi) W_{2n}\left(\frac{x}{\beta} - r + 1 - \frac{\xi}{\beta}, r \right) d\xi \right] \qquad (9)$$

The pressure field due to the wing alone can be determined as a pure wing problem in linear theory. Let $P_{W(W)}$ be the component of this field acting on the wing and $P_{B(W)}$ the component acting on the body. Let $P_{B(W)}$ be composed of a component due to infinite aspect ratio plus a component due to the difference between infinite and the actual aspect ratio, that is, a component due to the tip. Performing a Fourier analysis of the $P_{B(W)}$ field around the body section and indicating the part due to the wing tip with an asterisk, we obtain

$$\frac{P_{B(W)}}{(t_m/c_r)} = 2 \sum_{n=0}^{\infty} \left[p_{2n}(x) + p_{2n}^*(x) \right] \cos 2n\theta \qquad (10)$$

[redacted]

The factor of 2 has been introduced purely for later convenience, and the values of $p_{2n}(x)$ and $p_{2n}^*(x)$ thus represent only half the true Fourier amplitudes. The quantity $p_{2n}^*(x)$ can be thought of as due to the image system of line sources and sinks representing the tip when the wing pressure field is constructed of line pressure sources in accordance with reference 7.

The pressure due to the interference field is obtained in the same manner as in references 4 and 5, or analogously as that due to body distortion. Let the normal velocity induced at the body surface by the wing-alone field be Fourier analyzed around the body in a manner similar to the wing-alone pressure field so that

$$\frac{v_r}{V} = -\left(\frac{t_m}{c_r}\right) \sum_{n=0}^{\infty} \left[f_{2n}(x) + f_{2n}^*(x) \right] \cos 2n\theta \tag{11}$$

Equation (11) gives the virtual distortion of a cylindrical body necessary to conform to the wing-alone flow field. Since the cylindrical body is, in fact, not distorted by the wing flow field, it sets up an interference pressure field equal and opposite to that associated with the virtual distortion. This opposite effect also explains the use of a minus sign in equation (11). Analogous to equations (8) and (9), we obtain

$$\frac{P_{B(i)}}{(t_m/c_r)} = \frac{2}{\beta} \sum_{n=0}^{\infty} \left\{ f_{2n}(x) + f_{2n}^*(x) - \frac{1}{\beta} \int_0^x \left[f_{2n}(\xi) + f_{2n}^*(\xi) \right] W_{2n}\left(\frac{x-\xi}{\beta}, 1\right) d\xi \right\} \cos 2n\theta \tag{12}$$

$$\frac{P_{W(i)}}{(t_m/c_r)} = \frac{2}{\beta} \sum_{n=0}^{\infty} \left\{ \frac{f_{2n}(x - \beta r + \beta)}{\sqrt{r}} + \frac{f_{2n}^*(x - \beta r + \beta)}{\sqrt{r}} - \frac{1}{\beta} \int_0^{x-\beta r+\beta} \left[f_{2n}(\xi) + f_{2n}^*(\xi) \right] W_{2n}\left(\frac{x}{\beta} - r + 1 - \frac{\xi}{\beta}, r\right) d\xi \right\} \tag{13}$$

Drag of Body and Wing in Combination

The resultant pressure acting on the body of the combination is the sum of the pressure coefficients given by equations (8), (10), and (12). Let the body be distorted over the interval $0 \leq x \leq l$. Then the body in combination has the drag

$$\left(\frac{D}{q}\right)_{B(C)} = \int_0^l \int_0^{2\pi} \left[P_{B(d)} + P_{B(W)} + P_{B(i)}\right] r \frac{dr}{dx} d\theta \, dx \tag{14}$$

With r taken as unity, we obtain

$$\frac{(D/q)_{B(C)}}{(t_m/c_r)^2} = \frac{2}{\beta} \int_0^l dx \int_0^{2\pi} \sum_{m=0}^{\infty} \left[g_{2m}(x)\cos 2m\theta\right] \sum_{n=0}^{\infty} \left\{g_{2n}(x) + \beta p_{2n}(x) + \right.$$

$$\beta p_{2n}{}^*(x) + f_{2n}(x) + f_{2n}{}^*(x) - \frac{1}{\beta} \int_0^x \left[g_{2n}(\xi) + f_{2n}(\xi) + \right.$$

$$\left. \left. f_{2n}{}^*(\xi)\right] W_{2n}\left(\frac{x-\xi}{\beta}, 1\right) d\xi \right\} \cos 2n\theta \, d\theta \tag{15}$$

The total drag of the body in combination can be expressed as the sum of the drags of the various Fourier components since the components are orthogonal; that is, the pressures due to one component cause no drag by acting on the shapes of the other components.

$$\frac{(D/q)_{B(C)}}{(t_m/c_r)^2} = \sum_{n=0}^{\infty} \frac{(D/q)_{B(C)_{2n}}}{(t_m/c_r)^2} \tag{16}$$

Then for $n = 0$

$$\frac{(D/q)_{B(C)_0}}{(t_m/c_r)^2} = \frac{4\pi}{\beta} \int_0^l g_0(x) \left\{g_0(x) + \beta p_0(x) + \beta p_0{}^*(x) + f_0(x) + f_0{}^*(x) - \right.$$

$$\left. \frac{1}{\beta} \int_0^x \left[g_0(\xi) + f_0(\xi) + f_0{}^*(\xi)\right] W_0\left(\frac{x-\xi}{\beta}, 1\right) d\xi \right\} dx \tag{17}$$

[redacted]

and for $n \neq 0$

$$\frac{(D/q)_{B(C)_{2n}}}{(t_m/c_r)^2} = \frac{2\pi}{\beta}\int_0^l g_{2n}(x)\left\{g_{2n}(x) + \beta p_{2n}(x) + \beta p_{2n}^*(x) + f_{2n}(x) + f_{2n}^*(x) - \frac{1}{\beta}\int_0^x \left[g_{2n}(\xi) + f_{2n}(\xi) + f_{2n}^*(\xi)\right] W_{2n}\left(\frac{x-\xi}{\beta}, 1\right)d\xi\right\}dx \tag{18}$$

The pressure coefficient acting on the wing in combination is given by the sum of $P_{W(d)}$, $P_{W(W)}$, and $P_{W(i)}$. Consider the drag of the wing panel $D_{W(W)}$ known from wing-alone theory, and evaluate $D_{W(d)}$ and $D_{W(i)}$ as follows: Consider first the pressure components $2g_{2n}(x - \beta r + \beta)/\beta\sqrt{r}$ and $2f_{2n}(x - \beta r + \beta)/\beta\sqrt{r}$ which represent Ackeret pressures or two-dimensional linear-theory pressures attenuating inversely as the square root of r along the body characteristics. Including tip effects and considering both sides of both wing panels, we obtain for this component of the wing wave drag

$$\frac{(D/q)^{(1)}_{W(i+d)}}{(t_m/c_r)} = \frac{8}{\beta}\iint_{S_P}\sum_{n=0}^{\infty}\left[\frac{g_{2n}(x-\beta r+\beta)}{\sqrt{r}} + \frac{f_{2n}(x-\beta r+\beta)}{\sqrt{r}} + \frac{f_{2n}^*(x-\beta r+\beta)}{\sqrt{r}}\right]\frac{\partial z_u}{\partial x}\,dS_P \tag{19}$$

$$\frac{(D/q)^{(1)}_{W(i+d)}}{(t_m/c_r)^2} = \frac{8}{\beta}\sum_{n=0}^{\infty}\iint_{S_P}\left[\frac{g_{2n}(x-\beta r+\beta)}{\sqrt{r}} + \frac{f_{2n}(x-\beta r+\beta)}{\sqrt{r}} + \frac{f_{2n}^*(x-\beta r+\beta)}{\sqrt{r}}\right]c_r\,\frac{\partial\eta(x-\beta r+\beta, r)}{\partial x}\,dr\,d(x-\beta r+\beta) \tag{20}$$

It is convenient to integrate first outward along strips in the characteristic direction and then to sum the strips between the leading and trailing characteristics tangent to the wing plan form as shown in sketch (c).

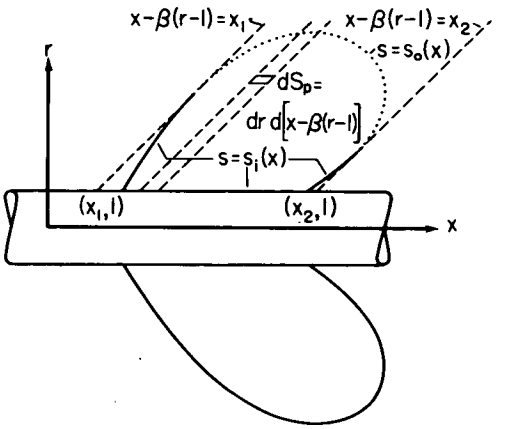

Sketch (c)

$$\frac{(D/q)^{(1)}_{W(i+d)}}{(t_m/c_r)^2} = \frac{8}{\beta}\sum_{n=0}^{\infty}\int_{x_1}^{x_2}\Big[g_{2n}(x-\beta r+\beta) + f_{2n}(x-\beta r+\beta) + f_{2n}^*(x-\beta r+\beta)\Big]d(x-\beta r+\beta)\int_{s_i}^{s_o} c_r\frac{\partial\eta(x-\beta r+\beta,r)}{\partial x}\frac{dr}{\sqrt{r}} \tag{21}$$

or

$$\frac{(D/q)^{(1)}_{W(i+d)}}{(t_m/c_r)^2} = \frac{8}{\beta}\sum_{n=0}^{\infty}\int_{x_1}^{x_2}\Big[g_{2n}(x) + f_{2n}(x) + f_{2n}^*(x)\Big]\int_{s_i}^{s_o} c_r\frac{\partial\eta(x,r)}{\partial x}\frac{dr}{\sqrt{r}}\,dx \tag{22}$$

Consider now that part of the drag due to the pressure disturbances lying behind the Mach cones on which they originated and represented by the integral forms in equations (9) and (13). This second component of the wing wave drag is

$$\frac{(D/q)^{(2)}_{W(i+d)}}{(t_m/c_r)^2} = -\frac{8}{\beta^2}\sum_{n=0}^{\infty}\iint_{S_P}\left\{\int_0^{x-\beta(r-1)}\Big[g_{2n}(\xi) + f_{2n}(\xi) + f_{2n}^*(\xi)\Big]W_{2n}\left(\frac{x}{\beta} - r + 1 - \frac{\xi}{\beta}, r\right)d\xi\right\} c_r\frac{\partial\eta}{\partial x}\,dS_P \tag{23}$$

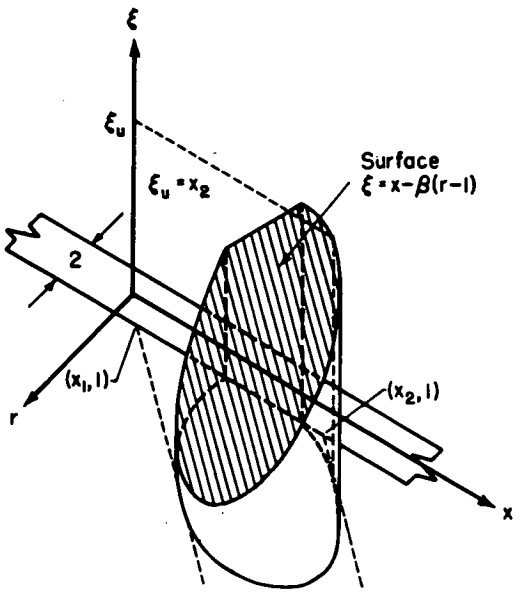

Sketch (d)

The volume of integration is shown in sketch (d). In this sketch the positive r direction has been reversed for clarity. Let us reverse the order of integration so that in the x,r,ξ space we integrate over a slab parallel to the x,r plane and then sum the slabs with respect to ξ. Since $W_{2n}(x,r) = 0$ if x is negative, there is obtained

$$\frac{(D/q)^{(2)}_{W(i+d)}}{(t_m/c_r)^2} = -\frac{8}{\beta^2}\sum_{n=0}^{\infty}\int_0^{\xi_u}\left[g_{2n}(\xi) + f_{2n}(\xi) + f_{2n}^*(\xi)\right]d\xi \iint_{S_P} W_{2n}\left(\frac{x}{\beta} - r + 1 - \frac{\xi}{\beta}, r\right) c_r \frac{\partial \eta}{\partial x}\, dr\, d(x - \beta r + \beta) \tag{24}$$

or

$$\frac{(D/q)^{(2)}_{W(i+d)}}{(t_m/c_r)^2} = -\frac{8}{\beta^2}\sum_{n=0}^{\infty}\int_0^{x_2}\left[g_{2n}(x) + f_{2n}(x) + f_{2n}^*(x)\right]dx \iint_{S_P} W_{2n}\left(\frac{\xi}{\beta} - r + 1 - \frac{x}{\beta}, r\right) c_r \frac{\partial \eta}{\partial \xi}\, dr\, d(\xi - \beta r + \beta) \tag{25}$$

The entire drag of the wing in the presence of the distorted body is thus

$$\frac{(D/q)_{W(C)}}{(t_m/c_r)^2} = \frac{(D/q)_{W(W)}}{(t_m/c_r)^2} + \frac{8}{\beta}\sum_{n=0}^{\infty}\int_{x_1}^{x_2}\left[g_{2n}(x) + f_{2n}(x) + f_{2n}^*(x)\right]dx$$

$$\int_{s_i}^{s_o} c_r \frac{\partial\eta(x,r)}{\partial x}\frac{dr}{\sqrt{r}} - \frac{8}{\beta^2}\sum_{n=0}^{\infty}\int_{o}^{x_2}\left[g_{2n}(x) + f_{2n}(x) + f_{2n}^*(x)\right]dx$$

$$\iint_{S_P} W_{2n}\left(\frac{\xi}{\beta} - r + 1 - \frac{x}{\beta}, r\right) c_r \frac{\partial\eta}{\partial\xi}\, dr\, d(\xi - \beta r + \beta) \qquad (26)$$

Body Shape for Minimum Drag and Drag Saving

In this section we will derive an integral equation for the body shape for minimum wave drag. As noted in the Introduction, the alternate method of Lomax and Heaslet also yields a solution for body shape for minimum wave drag. The two solutions, although not mathematically identical, are equal to the order of quasi-cylindrical theory. The solution by the alternate method as well as its relationship to the present method is described in Appendix C.

The drag of the combination can be expressed as the sum of the wing-alone drag plus the drag of a number of independent Fourier components. We can minimize the drag of any component or combination of components independently of the others; for instance, we can minimize the drag of the second component without altering the first component which controls the volume. The equation for the wave drag of the combination to be used in the minimization is

[redacted]

$$\frac{(D/q)_C}{(t_m/c_r)^2} = \frac{\pi}{\beta}\sum_{n=0}^{\infty}\lambda_n \int_0^l g_{2n}(x)\left\{g_{2n}(x) + \beta p_{2n}(x) + \beta p_{2n}{}^*(x) + f_{2n}(x) + f_{2n}{}^*(x) - \right.$$

$$\left.\frac{1}{\beta}\int_0^x \left[g_{2n}(\xi) + f_{2n}(\xi) + f_{2n}{}^*(\xi)\right] W_{2n}\left(\frac{x-\xi}{\beta}, 1\right) d\xi\right\} dx +$$

$$\frac{8}{\beta}\sum_{n=0}^{\infty}\int_0^l \left[g_{2n}(x) + f_{2n}(x) + f_{2n}{}^*(x)\right]\int_{s_i}^{s_o} c_r \frac{\partial\eta(x,r)}{\partial x}\frac{dr}{\sqrt{r}}\, dx +$$

$$\frac{(D/q)_{W(W)}}{(t_m/c_r)^2} - \frac{8}{\beta^2}\sum_{n=0}^{\infty}\int_0^l \left[g_{2n}(x) + f_{2n}(x) + f_{2n}{}^*(x)\right] dx$$

$$\iint_{S_P} W_{2n}\left(\frac{\xi}{\beta} - r + 1 - \frac{x}{\beta}, r\right) c_r \frac{\partial\eta}{\partial\xi}\, dr\, d(\xi - \beta r + \beta) \qquad (27)$$

The range of the integrals in the terms was increased from $x_1 \leq x \leq x_2$ to $0 \leq x \leq l$ with the help of simple properties of $W_{2n}(x,r)$ and $\eta(x,r)$. The constant λ_n is 4 for $n = 0$ and 2 for $n > 0$. In the minimization of the drag as given by the above formula, the condition is considered in which the shape of the indentation for the particular Fourier harmonic is at its value for minimum drag and then a variation $\delta g_{2n}(x)$ from this

shape is considered. The additional drag due to the variation, δD_C, is zero and is given as

$$\frac{\delta(D/q)_C}{(t_m/c_r)^2} = \frac{\pi}{\beta}\sum_{n=0}^{\infty}\lambda_n\int_0^l \delta g_{2n}(x)\left\{2g_{2n}(x) + \beta p_{2n}(x) + \beta p_{2n}{}^*(x) + f_{2n}(x) + \right.$$

$$\left. f_{2n}{}^*(x) - \frac{1}{\beta}\int_0^x \left[g_{2n}(\xi) + f_{2n}(\xi) + f_{2n}{}^*(\xi)\right] W_{2n}\left(\frac{x-\xi}{\beta}, 1\right)d\xi\right\} dx -$$

$$\frac{\pi}{\beta^2}\sum_{n=0}^{\infty}\lambda_n\int_0^l g_{2n}(x)dx\int_0^x \delta g_{2n}(\xi)W_{2n}\left(\frac{x-\xi}{\beta},1\right)d\xi +$$

$$\frac{8}{\beta}\sum_{n=0}^{\infty}\int_0^l \delta g_{2n}(x)dx\int_{s_i}^{s_o} c_r\frac{\partial\eta(x,r)}{\partial x}\frac{dr}{\sqrt{r}} - \frac{8}{\beta^2}\sum_{n=0}^{\infty}\int_0^l \delta g_{2n}(x)dx$$

$$\iint_{S_P} W_{2n}\left(\frac{\xi}{\beta} - r + 1 - \frac{x}{\beta}, r\right)c_r\frac{\partial\eta}{\partial\xi}\,dr\,d(\xi - \beta r + \beta) \qquad (28)$$

With the inversion of the following integral

$$\int_0^l g_{2n}(x)dx\int_0^x \delta g_{2n}(\xi)W_{2n}\left(\frac{x-\xi}{\beta},1\right)d\xi = \int_0^l \delta g_{2n}(x)dx\int_x^l g_{2n}(\xi)W_{2n}\left(\frac{\xi-x}{\beta},1\right)d\xi$$

(29)

[redacted]

equation (28) becomes

$$\frac{\delta(D/q)_C}{(t_m/c_r)^2} = \frac{\pi}{\beta}\sum_{n=o}^{\infty}\lambda_n\int_o^l \delta g_{2n}(x)\left\{2g_{2n}(x) + \beta p_{2n}(x) + \beta p_{2n}^*(x) + f_{2n}(x) + \right.$$

$$f_{2n}^*(x) - \frac{1}{\beta}\int_o^l g_{2n}(\xi)W_{2n}\left|\frac{\xi - x}{\beta}\right|d\xi - \frac{1}{\beta}\int_o^x \left[f_{2n}(\xi) + \right.$$

$$\left.\left. f_{2n}^*(\xi)\right]W_{2n}\left(\frac{x-\xi}{\beta},1\right)d\xi\right\}dx + \frac{8}{\beta}\sum_{n=o}^{\infty}\int_o^l \delta g_{2n}(x)$$

$$\left[\int_{s_i}^{s_o} c_r\frac{\partial\eta(x,r)}{\partial x}\frac{dr}{\sqrt{r}} - \frac{1}{\beta}\iint_{S_P} W_{2n}\left(\frac{\xi}{\beta} - r + 1 - \frac{x}{\beta}, r\right)\right.$$

$$\left.c_r\frac{\partial\eta}{\partial\xi}dr\, d(\xi - \beta r + \beta)\right]dx \qquad (30)$$

Now $\delta(D/q)_C$ must be zero to the first order and since $\delta g_{2n}(x)$ is arbitrary and not zero, we must have for each n

$$\frac{\pi}{\beta}\lambda_n\left\{2g_{2n}(x)+\beta p_{2n}(x)+\beta p_{2n}{}^*(x)+f_{2n}(x)+f_{2n}{}^*(x)-\frac{1}{\beta}\int_0^l g_{2n}(\xi)W_{2n}\left|\frac{x-\xi}{\beta}\right|d\xi-\right.$$

$$\left.\frac{1}{\beta}\int_0^x\left[f_{2n}(\xi)+f_{2n}{}^*(\xi)\right]W_{2n}\left(\frac{x-\xi}{\beta},1\right)d\xi\right\}+\frac{8}{\beta}\left[\int_{s_i}^{s_o}c_r\frac{\partial\eta(x,r)}{\partial x}\frac{dr}{\sqrt{r}}-\right.$$

$$\left.\frac{1}{\beta}\iint_{S_P}W_{2n}\left(\frac{\xi}{\beta}-r+1-\frac{x}{\beta},r\right)c_r\frac{\partial\eta}{\partial\xi}dr\,d(\xi-\beta r+\beta)\right]=0 \quad (31)$$

This integral equation defining the optimum body distortions for each Fourier component can be written

$$g_{2n}(x)=h_{2n}(x)+\frac{1}{2\beta}\int_0^l g_{2n}(\xi)W_{2n}\left|\frac{x-\xi}{\beta}\right|d\xi \quad (32)$$

wherein

$$h_{2n}(x)=-\frac{1}{2}\left[\beta p_{2n}(x)+\beta p_{2n}{}^*(x)+f_{2n}(x)+f_{2n}{}^*(x)\right]+\frac{4}{\pi\lambda_n}\left[\frac{1}{\beta}\iint_{S_P}W_{2n}\left(\frac{\xi}{\beta}-r+\right.\right.$$

$$\left.1-\frac{x}{\beta},r\right)c_r\frac{\partial\eta(\xi-\beta r+\beta,r)}{\partial\xi}dr\,d(\xi-\beta r+\beta)-\int_{s_i}^{s_o}c_r\frac{\partial\eta(x,r)}{\partial x}\frac{dr}{\sqrt{r}}\Bigg]+$$

$$\frac{1}{2\beta}\int_0^x\left[f_{2n}(\xi)+f_{2n}{}^*(\xi)\right]W_{2n}\left(\frac{x-\xi}{\beta},1\right)d\xi \quad (33)$$

The nonhomogeneous term $h_{2n}(x)$ must be evaluated for the particular wing under consideration, the values of $p_{2n}(x)$, $p_{2n}^*(x)$, $f_{2n}(x)$, and $f_{2n}^*(x)$ following from a knowledge of the wing-alone flow field. Equation (32) is then solved by numerical means to determine the best distortion of the body for the Fourier harmonic under consideration. The actual distortions are proportional to the wing thickness because of the use of quasi-cylindrical theory and the application of the boundary conditions on the $r = 1$ cylinder. The wing thickness must be sufficiently thin, therefore, for the distortions to be within the compass of quasi-cylindrical theory. For a wing of greater thickness an auxiliary condition can be imposed on the allowable magnitude of the distortion and the minimum problem resolved subject to such a condition in a manner similar to that of Lomax and Heaslet (ref. 3).

A simple rule for the drag saved can be determined by evaluating the drag of the combination at the minimum-drag condition. Under this condition the drag is

$$\frac{(D/q)_C}{(t_m/c_r)^2} = \frac{\pi}{\beta}\sum_{n=0}^{\infty}\lambda_n\int_0^1 g_{2n}(x)\left[-g_{2n}(x)+\frac{1}{\beta}\int_x^1 g_{2n}(\xi)W_{2n}\left(\frac{\xi-x}{\beta},1\right)d\xi\right]dx +$$

$$\frac{(D/q)_{W(W)}}{(t_m/c_r)^2} + \frac{8}{\beta}\sum_{n=0}^{\infty}\int_0^1\left[f_{2n}(x)+f_{2n}^*(x)\right]dx\int_{s_i}^{s_o} c_r\frac{\partial\eta(x,r)}{\partial x}\frac{dr}{\sqrt{r}} -$$

$$\frac{8}{\beta^2}\sum_{n=0}^{\infty}\int_0^1\left[f_{2n}(x)+f_{2n}^*(x)\right]dx\iint_{S_P} W_{2n}\left(\frac{\xi}{\beta}-r+\right.$$

$$\left.1-\frac{x}{\beta},r\right)c_r\frac{\partial\eta}{\partial\xi}\,dr\,d(\xi-\beta r+\beta) \qquad (34)$$

The last three terms represent the drag of the wing panels with a cylindrical body, in which case the drag of the panels is the total drag of

[redacted]

the winged part of the combination. The first term thus represents the drag saved. If the order of integration of this term is reversed, we obtain

$$\frac{(D/q)_S}{(t_m/c_r)^2} = -\frac{\pi}{\beta}\sum_{n=0}^{\infty}\lambda_n\int_0^l g_{2n}(x)\left[g_{2n}(x) - \frac{1}{\beta}\int_0^x g_{2n}(\xi)W_{2n}\left(\frac{x-\xi}{\beta},1\right)d\xi\right]dx$$

$$= -\frac{\pi}{\beta}\sum_{n=0}^{\infty}\lambda_n\int_0^l g_{2n}(x)h_{2n}(x)dx \qquad (35)$$

It is readily seen that the drag saving is simply the drag of the distorted body without any wing panels, and that this drag is the same whether the distorted body moves in one direction along its axis or in the other direction. If the combination is operated at a Mach number other than the design Mach number, the drag saving is less that that given by equation (35).

It is possible to build up the potential fields due to the addition of a quasi-cylindrical body to a wing, φ_i and φ_B, by distributing sources and multipoles along the x axis as well as by the $W_{2n}(x,r)$ method. Any set of solutions to the wave equation in cylindrical coordinates that is of the form of a function of x and r multiplied by $\cos 2n\theta$ can in principle be used for the purpose. In reference 4 a method is given of relating the body distortions to the multipole strengths for the particular set of solutions used therein. The same method is used in Appendix B to show the relationship between body distortion and multipole strength for the multipoles of reference 3. In Appendix C the equivalence between the quasi-cylindrical and multipole methods is used to derive the body shapes of a minimum-drag wing-body combination in a form amenable to analytical as well as numerical calculation.

II - CALCULATIVE EXAMPLE OF SWEPT-WING AND BODY COMBINATION WITH SONIC LEADING AND TRAILING EDGES

An interesting example of the general theory is the case of a swept-wing and body combination with sonic leading and trailing edges. By distorting the body properly it appears possible to reduce the drag rise that occurs as a swept-wing airplane approaches the Mach number for which its leading edge becomes sonic and thereby to increase the Mach number at which a given swept-wing airplane loses its sweepback effectiveness.

The supersonic area rule (refs. 8 and 9) gives an approximate idea of the shape of the distortion due to the axially symmetric harmonic.

As an example, a minimum-drag computation is made for two harmonics of the swept wing and body shown in sketch (e). The calculation is for $M = \sqrt{2}$. If a combination at some other Mach number is desired, it can be first transformed to $M = \sqrt{2}$ in accordance with Appendix D and then the answers should be transformed back to the original Mach number. The results of the calculation for swept wings with sonic edges are plotted in nondimensional form applicable to any Mach number. A biconvex airfoil section has been used with a thickness distribution given by

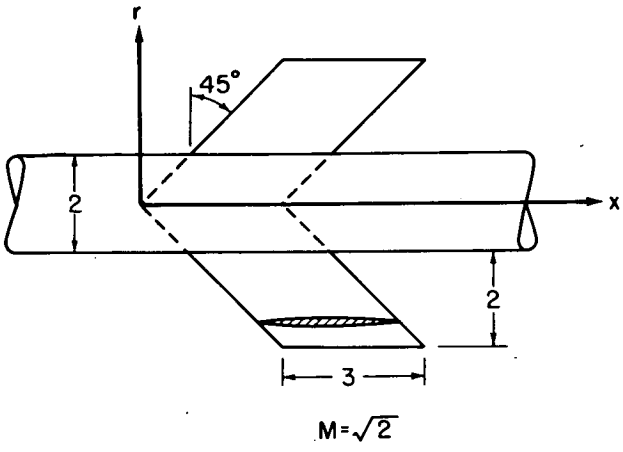

Sketch (e)

$$z_u = 2t_m\left(\frac{x-r}{c}\right)\left(1 - \frac{x-r}{c}\right)$$

$$= t_m\eta[x-(r-1), r] \qquad (36)$$

on the wing and $z_u = 0$ off the plan form. The first major step in the calculation is to evaluate the various components of $h_{2n}(x)$ as given by equation (33). The relative magnitudes of these components are in direct proportion to their importance in prescribing the proper shape for minimum drag so that considerable insight into the problem is obtained in this step. The second step is to solve the integral equation for the minimizing shapes, and the third step is to evaluate the drag saving, volume of cutout, pressure distributions, etc.

Velocity and Pressure Amplitude Functions

The first four terms of equation (33) relate to the pressure and normal velocity fields produced at the surface of the body by the wing-alone flow field. For the present example consider the wing alone to include the area blanketed by the body when the leading and trailing edges are extended as straight lines. The pressure and velocity fields of the wing alone can be built up by superimposing line pressure sources of the type given by R. T. Jones in reference 7. The u, v, and w fields of such a line source, as pictured in sketch (f),

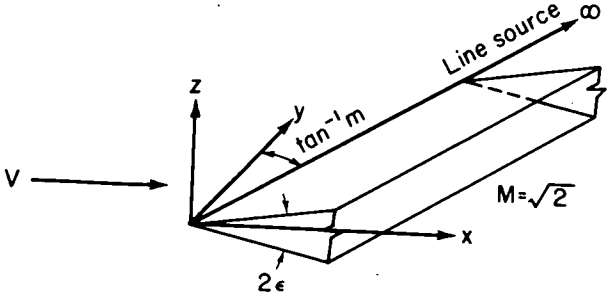

Sketch (f)

are given in reference 10 for $M = \sqrt{2}$ as

$$\frac{u}{V} = -\text{R.P.}\ \frac{m\epsilon}{\pi\sqrt{1-m^2}} \cosh^{-1} \frac{x'}{\sqrt{y'^2+z'^2}} \tag{37}$$

$$\frac{v}{V} = \text{R.P.}\ \frac{\epsilon}{\pi}\left[\frac{1}{\sqrt{1-m^2}} \cosh^{-1}\left(\frac{x'}{\sqrt{y'^2+z'^2}}\right) - \cosh^{-1}\frac{x}{\sqrt{y^2+z^2}}\right] \tag{38}$$

$$\frac{w}{V} = \text{R.P.}\ \frac{\epsilon}{\pi} \cos^{-1} \frac{yy'+z^2}{\sqrt{y^2+z^2}\sqrt{y'^2+z'^2}} \tag{39}$$

wherein

$$x' = x - my; \qquad y' = y - mx; \qquad z' = z\sqrt{1-m^2}$$

For a sonic leading edge, let m approach unity and obtain the limits of equations (37), (38), and (39) as

$$\frac{u}{V} = -\frac{\epsilon}{\pi}\frac{\sqrt{x^2-y^2-z^2}}{(x-y)} \tag{40}$$

$$\frac{v}{V} = \frac{\epsilon}{\pi}\left[\frac{\sqrt{x^2-y^2-z^2}}{(x-y)} - \cosh^{-1}\frac{x}{\sqrt{y^2+z^2}}\right] \tag{41}$$

$$\frac{w}{V} = \frac{\epsilon}{\pi} \cos^{-1}\left[\frac{y(y-x)+z^2}{(x-y)\sqrt{y^2+z^2}}\right] \tag{42}$$

From these equations the normal velocity and pressure distribution acting on the cylinder $y^2 + z^2 = 1$ can easily be determined. The velocity normal to the cylinder was computed for 15° intervals around the cylinder

[redacted]

and then Fourier analyzed using numerical methods for the pair of line sources 1-1 shown in sketch (g) as well as for a pair of tip sources 2-2. The coefficients so calculated correspond to the Fourier series

$$\frac{v_r}{V\epsilon} = f_{0_s}(x) + f_{2_s}(x)\cos 2\theta + \ldots \tag{43}$$

$$\frac{v_r^*}{V\epsilon} = f_{0_s}^*(x) + f_{2_s}^*(x)\cos 2\theta + \ldots \tag{44}$$

wherein the asterisk refers to the tip sources. The values of the Fourier coefficients are shown in figure 2. The constancy of the $f_{0_s}(x)$ coefficient is noteworthy since the normal velocity distribution varies with x. It is apparent that the tip has a minor influence.

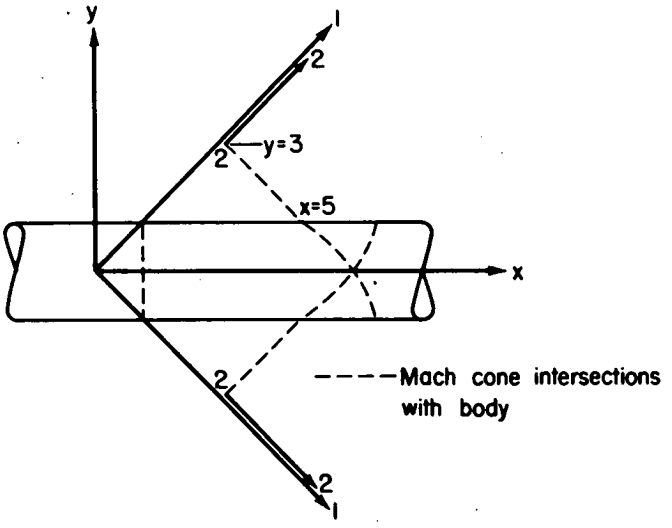

Sketch (g)

To obtain the velocity amplitude functions for the wing as a whole as defined by equation (11), it is necessary to superimpose the effects of the sources and sinks that form the wing in accordance with sketch (h). The effect of the infinite number of small sinks between the leading and trailing edges is summed by integration. The resultant values of $f_0(x)$, $f_2(x)$, $f_0^*(x)$, $p_0(x)$, $p_2(x)$, and $p_0^*(x)$ are given in figure 3.

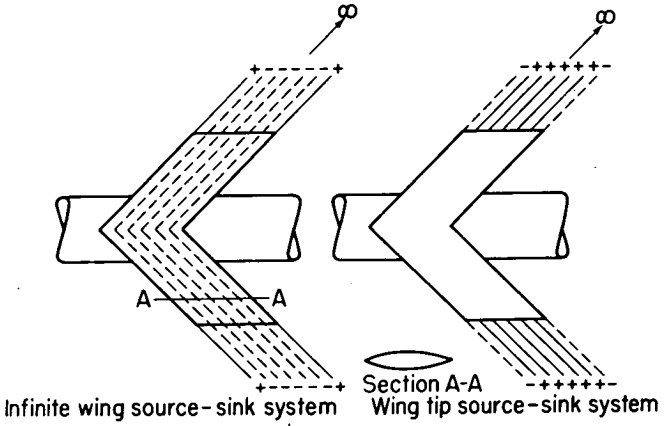

Sketch (h)

The main terms of equation (33) are readily determined. The final term involves numerical integration using the values of the $W_{2n}(x,r)$ functions in figure 1. The sixth term can be ascertained in closed form. Since from equation (36)

$$\eta(x - r + 1, r) = 2\left(\frac{x-r}{c}\right)\left(1 - \frac{x-r}{c}\right) \tag{45}$$

we obtain

$$\frac{\partial \eta(x,r)}{\partial x} = \frac{2}{c}\left[1 - \frac{2(x-1)}{c}\right] \tag{46}$$

Thus

$$\int_{s_i}^{s_o} c\,\frac{\partial \eta(x,r)}{\partial x}\,\frac{dr}{\sqrt{r}} = 4\left[1 - \frac{2(x-1)}{c}\right](\sqrt{s} - 1) \tag{47}$$

The term involving a double integral can be reduced to a single integral with the aid of equation (46)

$$\iint_{S_P} W_{2n}(\xi - r + 1 - x, r)\, c\,\frac{\partial \eta}{\partial \xi}(\xi - r + 1, r)\,dr\,d(\xi - r + 1)$$

$$= 2\iint_{S_P} W_{2n}(\xi - r + 1 - x, r)\left[1 - \frac{2(\xi - r)}{c}\right]dr\,d(\xi - r + 1)$$

$$= 2\int_1^{c+1}\left[1 - \frac{2(\xi - r)}{c}\right]d(\xi - r + 1)\int_1^{s} W_{2n}(\xi - r + 1 - x, r)\,dr$$

$$= 2\int_0^{c}\left(1 - \frac{2\xi}{c}\right)d\xi\int_1^{s} W_{2n}(\xi + 1 - x, r)\,dr \tag{48}$$

With the following definition

$$\Gamma_{2n}(x,s) = \int_1^{s} W_{2n}(x,r)\,dr \tag{49}$$

[redacted]

we achieve the desired result

$$\iint_{S_P} W_{2n}(\xi - r + 1 - x, r)\, c\, \frac{\partial \eta(\xi - r + 1, r)}{\partial \xi}\, dr\, d(\xi - r + 1)$$

$$= 2\int_0^c \left(1 - \frac{2\xi}{c}\right) \Gamma_{2n}(\xi - x + 1, s)\, d\xi \quad (50)$$

Solutions of Integral Equations for First Two Harmonics

The solutions of the integral equations represented by equation (32) have been obtained both by iteration and by simultaneous equations. If a first approximation to $g_{2n}(x)$ is known, say $g_{2n}^{(o)}(x)$, then a second approximation can be determined from the integral equation as

$$g_{2n}^{(1)}(x) = h_{2n}(x) + \frac{1}{2}\int_0^l g_{2n}^{(o)}(\xi) W_{2n}|x-\xi|\, d\xi \quad (51)$$

The process is repeated until it converges (or diverges). The convergence is greatly aided by a close first approximation. If a means of solving many simultaneous algebraic equations is at hand, the integral equation can be expressed as a number of simultaneous equations by writing the integral approximately as a summation. The more equations, the more accurate the answer. The rate of convergence is decreased by increasing the interval $0 \leq x \leq l$ or by increasing the order of the harmonic.

For the $n = o$ harmonic the solution was started by using $h_o(x)$ as a first approximation. The component terms of $h_o(x)$ are shown in figure 4. It is clear that the terms $f_o(x)$ and $p_o(x)$ are equal and opposite and the tip effects are small, so that the effect of the body distortions sending waves directly along the Mach cones is the dominant effect. This fact leads subsequently to a simple approximate theory. In the first calculation, the body was distorted only over the interval of the root chord. The subsequent approximations to $g_o(x)$ were obtained by iteration in accordance with the equation

$$g_o^{(j+1)}(x) = h_o(x) + \frac{1}{2}\int_1^{c+1} g_o^{(j)}(\xi) W_o|x-\xi|\, d\xi \quad (52)$$

[redacted]

The successive approximations converge so rapidly as shown by figure 5 that the initial approximation could have been used as the basis of a good approximate solution. In the second calculation, the possibility of distorting the body in front of the wing was considered with the result that the calculated distortion here is very close to zero, as shown by figure 6. For a general wing this corresponds to no distortion in front of the Mach rhombus enclosing the wing, a condition that follows readily from a consideration of momentum transfer through a large volume enclosing the combination. The effect of distorting the body downstream of the wing was investigated with the result that some distortion in this region is effective in further reducing the drag. However, the additional gain calculated for the present example is small. Thus, the significant interval for the purpose of the present example is the root chord, and no large change in the shape for minimum drag occurs over the interval of the root chord by considering a distortion interval greater than the root chord.

A solution for the integral equation for $n = 1$ was attempted in the same way as that for $n = 0$, but it was soon apparent that the rate of convergence was relatively slow. For this reason a better initial approximation was sought by solving a system of 11 simultaneous algebraic equations using the trapezoidal rule to evaluate the integral. The approximation so obtained is shown as $g_2^{(0)}(x)$ in figure 7. Several iterations then produced convergence.

Body Shape, Drag Saving, and Pressure Distributions

The solutions to the integral equations, $g_0(x)$ and $g_2(x)$, give the shape of the body for two harmonics from the integral of equation (1).

$$\frac{r_B}{a} = 1 + (t_m/c)\int_0^x g_0(\xi)d\xi + (t_m/c)\cos 2\theta \int_0^x g_2(\xi)d\xi \qquad (53)$$

The shapes of the indentations for the $n = 0$ and $n = 1$ harmonics at the wing-body junctures are shown in figure 8 for unit wing thickness. It is to be noted that the $n = 0$ indentation is similar to the wing profile. However, because of the finite chord length, the indentation does not come up to the full body radius at the wing trailing edge, a fact in accordance with the supersonic area rule. This point will be further elucidated when we consider effects of plan form on the $n = 0$ indentation. The $n = 1$ indentation is much larger than that for $n = 0$, an effect that tends to discourage the use of the higher harmonics. For the 5-percent-thick wing postulated, the indentation due to the second harmonic is so large that the assumption of a quasi-cylindrical body is

[redacted]

being stretched. The body cross section given by equation (53) incorporating both harmonics is shown in figure 9. The change in shape behind the trailing edge does not contribute much to the drag reduction as will be discussed later, and we therefore have the alternatives of incorporating the $n = 0$ afterbody, $n = 1$ afterbody, the afterbody using two harmonics, or a cylindrical afterbody as in figure 9. The percentage of the wing volume removed up to the trailing edge is 69 percent and up to the end of the Mach rhombus ($x = 8$) about 101 percent. Body volume is removed only by the $n = 0$ harmonic.

The slope of the indentation at the wing leading edge can be determined from the integral equation with the aid of the fact that $g_{2n}(x)$ must be nearly zero in front of the Mach rhombus (see Appendix C). The discontinuities in $g_{2n}(x)$ must coincide with the known discontinuities of $h_{2n}(x)$ at $x = 1$ because the integral of equation (32) is continuous. Hence,

$$g_{2n}(1^+) = h_{2n}(1^+) - h_{2n}(1^-) \tag{54}$$

The only term contributing to the discontinuity is the next to the last term of equation (33). With the help of equation (47), we obtain

$$g_{2n}(1^+) = -\frac{16}{\pi\lambda_n}(\sqrt{s} - 1) \tag{55}$$

Since each harmonic contributes a finite amount, the indentation for all the harmonics is initially radial in the $\theta = 0$ and $\theta = \pi$ planes.

The net drag saving due to body distortion has been computed by evaluating the drag of the distorted body alone in accordance with equation (35) and also from the pressure distributions acting on wing and body in combination. The distributions of the drag along the wing panels due to two harmonics of interference and distortion, shown in figure 10, have been integrated to obtain the net panel drags. The drags of the panels and body in combination for various conditions are summarized in sketch (i) which is to be studied in conjunction with

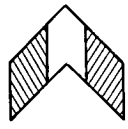

(1) Exposed panels of wing alone

$\frac{\beta C_D}{(t_m/c)^2}$

	Panels	Body
A	7.67	0

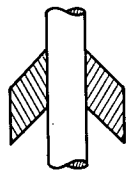

(2) Wing-cylindrical-body combination

	Panels	Body	Harmonics
A+B	5.48	0	n=0
A+B+C	5.67	0	n=0,1

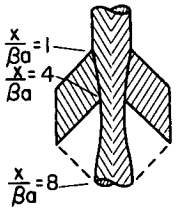

(3) Wing-distorted-body combination

	Panels	Body	Panels and body	Harmonics and intervals of distortion
A+B+C+D	3.60	.79	4.39	n=0, $1 \le \frac{x}{\beta a} \le 8$
A+B+C+D+E	-.49	2.61	2.12	n=0, $1 \le \frac{x}{\beta a} \le 8$
				n=1, $1 \le \frac{x}{\beta a} \le 4$

Sketch (i)

figure 10. Part (1) of the sketch shows the drag with the panels as part of the wing alone. Part (2) of the sketch illustrates how the addition of the cylindrical body has the effect of reducing the panel drag in the proportion 7.67 to 5.67. (It has been assumed that the interference drag for harmonics higher than the $n = 1$ harmonic is negligible.) Part (3) of the sketch shows the drag saving due to two harmonics of distortion. Incorporating the $n = 0$ distortion into the body reduces the drag of the combination by 22 percent (of 5.67) and the addition of the $n = 1$ harmonic has the effect of reducing the drag of the combination another 42 percent for a total of 64 percent. It is to be noted that distorting the body has the effect of reducing the drag of the wing in the presence of the body while increasing the drag of the body in the presence of the wing. The wing has negative wave drag when two harmonics of distortion are incorporated into the body. The net gain in drag is the result of reducing the wing-panel drag about twice as much as the drag of the body is increased. It is interesting that the section drag coefficients given by figure 10 for the harmonics of interference and distortion attenuates along the characteristics approximately inversely as the square root of the radius, so that drag savings can be realized for aspect ratios greater than that of the present example.

On the body the drag loading can be defined from equations (17) and (18) as

$$\frac{\frac{d}{dx}\left(\frac{D}{qS_W}\right)_{B(C)}}{(t_m/c)^2} = \sum_{n=0}^{\infty} \frac{\pi\lambda_n g_{2n}(x)}{S_W} \left\{ g_{2n}(x) + p_{2n}(x) + p_{2n}^*(x) + f_{2n}(x) + f_{2n}^*(x) - \int_0^x \left[g_{2n}(\xi) + f_{2n}(\xi) + f_{2n}^*(\xi) \right] W_{2n}(x-\xi)\,d\xi \right\} \qquad (56)$$

This quantity, plotted in figure 11, for the $n = 0$ and $n = 1$ harmonics, shows the distribution of drag along the body. This drag results from the pressure field arising from the body distortion and by distorting the body in an existing pressure field. It is noteworthy that extending the interval of distortion aft of the wing trailing edge causes only minor reductions in wave drag for the first harmonic. An approximate calculation shows this also to be true for the second harmonic.

The pressure distributions acting on wing and body both in combination can be readily determined, the distribution in the wing-body juncture

[redacted]

being given by

$$\frac{P}{(t_m/c)} = 2 \sum_{n=0}^{\infty} \left(\left\{ f_{2n}(x) + f_{2n}^*(x) - \int_0^x \left[f_{2n}(\xi) + f_{2n}^*(\xi) \right] W_{2n}(x - \xi) d\xi \right\} + \left[g_{2n}(x) - \int_0^x g_{2n}(\xi) W_{2n}(x - \xi) d\xi \right] + \left[p_{2n}(x) + p_{2n}^*(x) \right] \right) \quad (57)$$

The first component represents the effect of interference between wing panels and cylindrical body, the second component the effect of body distortion, and the third component the effect of the wing-alone field. The pressure distribution at the wing-body juncture for a cylindrical body is shown in figure 12(a). The wing-alone component of this pressure distribution has an infinity at the leading edge of the wing-body juncture. Because the body is a perfect reflection plane as far as this point is concerned, the pressure coefficient is the same as that at the apex of the wing alone, namely, $8/\pi$. The finite contributions of a finite number of harmonics of interference cannot overcome this infinity. However, we can easily establish the curve for the combination near the leading edge by fairing it into the known value. It is to be noted that the resultant pressure distribution has a favorable pressure gradient for the boundary layer. In figure 12(b) the pressure distribution for a distorted body has been determined by adding the pressures due to two harmonics of distortion to those for the cylindrical body. The resulting distribution has an unfavorable gradient. The effects at the wing-body juncture are typical of the wing as a whole since the pressure distributions on the span are essentially those of the root chord with an inverse variation as the square root of the radius (fig. 13). They are also typical of the body since they are simply multiplied by a $\cos 2n\theta$ factor. For a 5-percent-thick wing the complete pressure field at the wing-body juncture shows a pressure-coefficient rise from about -0.20 at the leading edge to about 0.25 at the trailing edge. This rise of $\Delta p/q = 0.45$ ($\Delta p/p = 0.63$) is less than the sudden pressure rise, $\Delta p/p$, of 0.9 necessary to separate a turbulent boundary layer as given by Bogdonoff and Kepler (ref. 11). It is thus probable that turbulent separation will not occur.

Approximate Solutions for Axially Symmetric Harmonic; Effect of Plan Form

On the basis of the relative magnitude of various terms of $h_o(x)$ in the integral equation for $g_o(x)$, equation (32), it is possible to obtain simple approximate solutions for the indentation shape and drag saving

for the $n = 0$ harmonic. The relative magnitude of the various terms depends primarily on the wing chord, or more specifically on $c/\beta r$, so that a short-chord theory and a medium-chord theory can be distinguished. In the analysis we will confine the indentation to the root chord and let βA_E be unity or greater so that no tip effects occur. The Mach number need not be $\sqrt{2}$ although the analysis is carried out for this Mach number. Under these conditions the effects of interference and the wing-alone pressure field represented by $f_o(x)$ and $p_o(x)$ are equal and opposite for this particular case, and equations (32) and (33) can be rewritten

$$g_o(x) = h_o(x) + \frac{1}{2}\int_o^c g_o(\xi)W_o|x-\xi|d\xi \tag{58}$$

$$h_o(x) = h_{o_1}(x) + h_{o_2}(x) + h_{o_3}(x) \tag{59}$$

with

$$h_{o_1}(x) = -\frac{4}{\pi\lambda_o}\int_{s_i}^{s_o} c\,\frac{\partial\eta(x,r)}{\partial x}\frac{dr}{\sqrt{r}} \tag{60}$$

$$h_{o_2}(x) = \frac{4}{\pi\lambda_o}\iint_{S_P} W_o(\xi - r + 1 - x, r)c\frac{\partial\eta(\xi - r + 1, r)}{\partial\xi}\,dr\,d(\xi - r + 1) \tag{61}$$

$$h_{o_3}(x) = \frac{1}{2}\int_o^x f_o(\xi)W_o(x - \xi)d\xi \tag{62}$$

The components of $h_o(x)$ involving the $W_{2n}(x,r)$ functions are concerned with departure of the pressures due to body indentations from the values that would be calculated by linear two-dimensional theory, and as such these components assume importance for medium to long chord lengths only.

Short-chord theory.- By neglecting $h_{o_2}(x)$ and $h_{o_3}(x)$ compared to $h_{o_1}(x)$, we obtain an approximate simple theory that represents the solution for vanishing chord length. Under this assumption the pressures acting on both body and wing are simply the linear-theory two-dimensional pressures based on the body distortion attenuated inversely as the square root of the radius. This simple physical model contains the primary

features of the flow due to the n = 0 harmonic, and the medium-chord approximation can be considered a slight modification of the simple model to account for three-dimensional effects on the pressure field. On the basis of the short-chord approximation, equations (58) to (62) yield

$$g_o(x) = h_o(x) = -\frac{1}{\pi}\int_1^s c\,\frac{\partial \eta(x,r)}{\partial x}\,\frac{dr}{\sqrt{r}} \tag{63}$$

Utilizing the result of equation (47), we obtain

$$\left.\frac{\partial r}{\partial x}\right]_{r=1} = \left(\frac{t_m}{c}\right) g_o(x) = -\left(\frac{4}{\pi}\right)\left(\frac{t_m}{c}\right)\left[1 - \frac{2(x-1)}{c}\right](\sqrt{s}-1) \tag{64}$$

and

$$\int_1^{r_B} dr = -\frac{4}{\pi}\left(\frac{t_m}{c}\right)(\sqrt{s}-1)\int_1^x \left[1 - \frac{2(x-1)}{c}\right] dx \tag{65}$$

Thus the shape of the indentation is given as

$$(1 - r_B) = \frac{4}{\pi}\, t_m(\sqrt{s}-1)\left(\frac{x-1}{c}\right)\left(1 - \frac{x-1}{c}\right) = \frac{2t_m}{\pi}(\sqrt{s}-1)\eta(x,1) \tag{66}$$

The shape of the indentation is similar to the wing section, but the volume of the indentation is usually less than the volume of the wing. In fact the ratio of indentation volume to wing volume is

$$\frac{V_i}{V_W} = \frac{\sqrt{s}-1}{s-1} \tag{67}$$

The volume ratio decreases as the span increases although the actual volume removed increases.

[redacted]

The drag saving calculated using equation (35) is

$$(D/q)_S = -\left(\frac{t_m}{c}\right)^2 (4\pi) \int_1^{c+1} g_o^2(x)\,dx \tag{68}$$

Expressed as a drag coefficient based on the area of the wing panels, the drag saving is

$$\frac{C_{D_S}}{(t_m/c)^2} = \frac{(D/qS_W)_S}{(t_m/c)^2} = -\frac{32}{3\pi}\frac{(\sqrt{s}-1)}{(\sqrt{s}+1)} \tag{69}$$

The coefficient of drag saving thus increases as the span increases but so does the drag of the wing alone. The effect of chord length will subsequently be discussed.

Medium-chord theory.- It was possible by neglecting three-dimensional effects to obtain very simple results for the first harmonic. However, for longer chord length than those to which the simple theory applies, account must be taken of the terms containing $W_{2n}(x,r)$ functions. The value of $h_{o_1}(x)$ remains as before. In the evaluation of $h_{o_2}(x)$ a simple assumption permits an approximate determination to be made readily. This assumption, expressed in physical terms, states that the three-dimensional effects represented by the $W_o(x,r)$ function themselves attenuate along the body characteristic in accordance with a simple approximation similar to that for the two-dimensional effects. Mathematically the approximation can be expressed as

$$W_o(x,r) \approx W_o(x,1)\frac{W_o(0,r)}{W_o(0,1)} \tag{70}$$

The validity of the assumption can be measured by how closely the quantity $W_o(x,r)W_o(0,1)/W_o(0,r)$ is invariant to changes in r. A plot of this quantity for various values of r is given in figure 14 to show that the approximation is a good one. The value of $W_{2n}(0,r)$ obtained from Laplace transform theory is

$$W_{2n}(0,r) = \frac{16n^2+3}{8\sqrt{r}} - \frac{16n^2-1}{8r^{3/2}} \tag{71}$$

[redacted]

so that

$$W_o(x,r) \approx \frac{W_o(x,1)}{4}\left(\frac{3}{r^{1/2}} + \frac{1}{r^{3/2}}\right) \tag{72}$$

From equation (72) we obtain the result

$$h_{o_2}(x) = \frac{8}{\pi\lambda_o}\int_o^c \int_1^s \frac{W_o(\eta - x + 1,1)}{8W_o(0,1)}\left(\frac{3}{r^{1/2}} + \frac{1}{r^{3/2}}\right)\left(1 - \frac{2\eta}{c}\right) dr\, d\eta \tag{73}$$

Integration yields

$$h_{o_2}(x) = \frac{(\sqrt{s} - 1)(3\sqrt{s} + 1)}{\pi\sqrt{s}}\left\{\left[1 - \frac{2(x-1)}{c}\right]Y(c - x + 1) - \frac{2}{c}Z(c - x + 1)\right\};$$

$$1 \le x \le c + 1 \tag{74}$$

with the following simple numerical quantities given in figure 15:

$$Y(x) \equiv \int_o^x W_o(\xi)d\xi; \qquad r = 1 \tag{75}$$

$$Z(x) \equiv \int_o^x \xi W_o(\xi)d\xi; \qquad r = 1 \tag{76}$$

Likewise the value $h_{o_3}(x)$ with the help of

$$f_o(\xi) = -\frac{4}{\pi}\left[1 - \frac{2(\xi - 1)}{c}\right]; \quad 1 \le \xi \le c + 1 \tag{77}$$

can easily be expressed in terms of the foregoing numerical quantities as

$$h_{o_3}(x) = -\frac{2}{\pi}\left\{\left[1 - \frac{2(x-1)}{c}\right]Y(x - 1) + \frac{2}{c}Z(x - 1)\right\} \tag{78}$$

With a good approximation to $h_o(x)$ including three-dimensional effects, we can now solve the integral equation for the body shape. In

evaluating the integral we will approximate $g_o(x)$ by $h_o(x)$ and apply the trapezoidal rule to the interval $1 \leq x \leq c + 1$ broken into n parts of length c/n. Then

$$g_o(x_i) = h_o(x_i) + \frac{c}{2n} \sum_{j=o}^{n} \mu_j h_o(\xi_j) W_o|x_i - \xi_j| \tag{79}$$

where

$$\left.\begin{aligned} \xi_j &= 1 + \frac{cj}{n} \\ \mu_j &= \frac{1}{2}; \qquad j = 0,n \\ \mu_j &= 1; \qquad 0 < j < n \end{aligned}\right\} \tag{80}$$

The example already solved exactly for the interval $1 \leq x \leq c + 1$ is used in figure 16 to measure the accuracy of the approximate methods. For a chord-radius ratio of 3 the short-chord theory is already inaccurate but the medium-chord theory is in good agreement with the exact solution. Some improvement in accuracy can be obtained by iterating equation (79), but for a more exact solution a better integration formula is needed - one recognizing the slope discontinuity in $W_o|x_i - \xi_i|$ at $x_i = \xi_i$. The drag saving evaluated by the trapezoidal rule is

$$C_{D_S} = \left(\frac{D}{qS_W}\right)_S = -\frac{4\pi c}{nS_W}\left(\frac{t_m}{c}\right)^2 \sum_{j=o}^{n} \mu_j g_o(x_j) h_o(x_j) \tag{81}$$

Effect of chord-radius and semispan-radius ratios.- The effect of the geometric variables on the body indentation, drag saving, and volume of indentation have been calculated using the medium-chord theory to study the limitations of the short-chord theory. The drag saving is shown in figure 17 as a function of s/a and $c/\beta a$. The saving increases as the wing span increases and increases slightly as the chord increases. The short-chord theory gives a good rough measure of the drag saving up to values of $c/\beta a$ of the order of 4. The volume of the indentation as a fraction of the wing volume is given in figure 18. It is seen that short-chord theory gives accurate volumes only for very short chords. Some actual indentation shapes are given in figure 19. The main feature of the shapes is that for the longer chord lengths the indentations do not return to the original radius. This result would be predicted by the

[redacted]

supersonic area rule. Those that do tend to return do not have nearly as much volume as the wing panels. Thus, as the design Mach number is increased from unity, the leading edge remaining sonic, the body volume to be removed decreases from the wing volume at $M = 1$ to a fraction of the wing volume at higher supersonic speeds. If distortion is made over the entire length of the Mach rhombus, the transonic area rule gives an indentation volume equal to the volume of the wing panels at $M = 1$ and the present method gives 101 percent of that volume at $M = \sqrt{2}$.

CONCLUDING REMARKS

The Nielsen-Pitts theory of wing-body interference has been applied to the problem of minimizing the wave drag of wing-body combinations by utilizing radial body distortion. The method, applicable to combinations with quasi-cylindrical bodies and horizontal planes of symmetry, deals directly with pressure distributions and body shapes. An integral equation is derived for the body shape for minimum drag for each Fourier component of the radial body distortion. To demonstrate the use of the method, it is applied to the wave-drag reduction of a 45° swept-wing and body combination utilizing a wing chord of three body radii and a span of six body radii. The leading and trailing edges are taken as sonic, and the wing section is biconvex. The numerical results for this example support the following statements:

1. The axially symmetric harmonic of body distortion causes a reduction in wave drag of about 22 percent of the drag of the wing panels on the undistorted body while the second harmonic causes a further reduction of 42 percent.

2. The over-all wave-drag reduction is the result of reducing the wing-panel drag by about twice as much as the body drag is increased. In fact, with two harmonics the wave drag of the panels is approximately zero.

3. The axially symmetric harmonic yields results qualitatively in accordance with the supersonic area rule in that the body indentation does not return to the full body radius at the trailing edge of the wing-body juncture. The volume of indentation is only about two thirds of the wing volume for an interval of distortion of the root chord.

4. The maximum distortion of the cross section at the wing-body juncture due to the second harmonic is about five times that due to the axially symmetric harmonic although no volume is removed by the second harmonic. This limits the wing thickness for which the second harmonic can be fully utilized to about 5 percent or less.

5. The interval over which the body distortion was effective in producing reduction in wave drag is that of the root chord although some further small saving could be obtained by distorting the afterbody.

6. The pressure distributions produced on the wing by body distortion, although favorable for the wave drag, are unfavorable for the boundary layer.

7. A very simple short-chord theory can be obtained for the axially symmetric harmonic by neglecting three-dimensional body effects. An approximate treatment of these effects yields a simple medium-chord theory.

Ames Aeronautical Laboratory
National Advisory Committee for Aeronautics
Moffett Field, Calif., Feb. 7, 1955

[redacted]

APPENDIX A

PRESSURE FIELD DUE TO DISTORTED BODY AT ANY SUPERSONIC SPEED

Let us determine the pressure field due to a body distorted in accordance with equation (1)

$$\left.\frac{\partial r}{\partial x}\right]_{r=1} = \left(\frac{t_m}{c_r}\right) \sum_{n=0}^{\infty} g_{2n}(x) \cos 2n\theta \tag{A1}$$

We will consider $M = \sqrt{2}$ for the moment. The potential φ_B is to satisfy equation (A1) on the body and to fulfill the wave equation. By analogy with equations (12) and (16) of reference 4,

$$\varphi_B = V \left(\frac{t_m}{c_r}\right) L^{-1} \sum_{n=0}^{\infty} \frac{G_{2n}(s) K_{2n}(sr)}{s K_{2n}'(s)} \cos 2n\theta \tag{A2}$$

wherein

$$G_{2n}(s) = L[g_{2n}(x)] \tag{A3}$$

and $K_{2n}(s)$ is the modified Bessel function of the second kind. For the case $r = 1$ it was possible in reference 4 to express the inversion of equation (A2) in terms of characteristic functions independent of the shape of the bumps of the body. Thus in terms of the characteristic functions

$$W_{2n}(x) \equiv L^{-1}\left[\frac{K_{2n}(s)}{K_{2n}'(s)} + 1\right] \tag{A4}$$

it was shown that on the body

$$P = -\frac{2(\partial\varphi/\partial x)}{V} = 2\left(\frac{t_m}{c_r}\right) \sum_{n=0}^{\infty} \left[g_{2n}(x) - \int_0^x g_{2n}(\xi) W_{2n}(x - \xi) d\xi\right] \cos 2n\theta \tag{A5}$$

[redacted]

It is possible to determine the pressure at any point off the body in a manner similar to that for points on the body. This is accomplished by generalizing the characteristic functions to functions of two variables

$$W_{2n}(x,r) \equiv L^{-1}\left[e^{s(r-1)}\frac{K_{2n}(sr)}{K_{2n}'(s)} + \frac{1}{\sqrt{r}}\right] \tag{A6}$$

In Laplace transform notation the pressure coefficient is

$$P = -2\left(\frac{t_m}{cr}\right)\sum_{n=0}^{\infty} G_{2n}(s)\frac{K_{2n}(sr)}{K_{2n}'(s)}\cos 2n\theta$$

$$= -2\left(\frac{t_m}{cr}\right)\sum_{n=0}^{\infty} e^{-s(r-1)}G_{2n}(s)\left[e^{s(r-1)}\frac{K_{2n}(sr)}{K_{2n}'(s)} + \frac{1}{\sqrt{r}} - \frac{1}{\sqrt{r}}\right]\cos 2n\theta \tag{A7}$$

With the aid of the following equalities from Laplace transform theory

$$L^{-1}\left[e^{-s(r-1)}G_{2n}(s)\right] = g_{2n}(x - r + 1) \tag{A8}$$

$$L^{-1}\left[\frac{K_{2n}(sr)}{K_{2n}'(s)} + \frac{e^{-s(r-1)}}{\sqrt{r}}\right] = W_{2n}(x - r + 1, r) \tag{A9}$$

$$L^{-1}G_{2n}(s)\left[\frac{K_{2n}(sr)}{K_{2n}'(s)} + \frac{e^{-s(r-1)}}{\sqrt{r}}\right] = \int_0^{x-r+1} g_{2n}(\xi)W_{2n}(x - r + 1 - \xi, r)\,d\xi \tag{A10}$$

the final result for the pressure field on or off the body is

$$P = 2\left(\frac{t_m}{cr}\right)\sum_{n=0}^{\infty}\left[\frac{g_{2n}(x-r+1)}{\sqrt{r}} - \int_0^{x-r+1} g_{2n}(\xi)W_{2n}(x - r + 1 - \xi, r)\,d\xi\right]\cos 2n\theta \tag{A11}$$

[redacted]

For any Mach number the pressure coefficient is

$$P = \frac{2}{\beta}\left(\frac{t_m}{c_r}\right)\sum_{n=0}^{\infty}\left[\frac{g_{2n}(x-\beta r+\beta)}{\sqrt{r}} - \frac{1}{\beta}\int_0^{x-\beta r+\beta} g_{2n}(\xi)W_{2n}\left(\frac{x}{\beta}-r+1-\frac{\xi}{\beta},r\right)d\xi\right]\cos 2n\theta \tag{A12}$$

In this equation the functions $g_{2n}(x)$ are taken to be the actual amplitudes of the body distortion and do not depend on Mach number. If the combination is distorted as in the Prandtl-Glauert transformation (see Appendix D), then the $g_{2n}(x)$ functions will change with Mach number. To make computations using equation (A12) it is necessary to evaluate the integral numerically using tabulated or plotted values of $W_{2n}(x,r)$. Plots of $W_0(x,r)$ and $W_2(x,r)$ sufficient for the purposes of this report are included in figure 1.

APPENDIX B

RELATIONSHIP BETWEEN SHAPE OF QUASI-CYLINDRICAL BODY AND STRENGTHS OF AXIAL MULTIPOLE DISTRIBUTIONS

The method used in this report deals exclusively with the flow field external to the wing-body combination and requires no continuation of the solution inside the body. However, it is intuitively clear that any quasi-cylindrical flow can be built up by superimposing distributions of sources and multipoles along the axis of the body. For the particular set of sources and multipoles used in reference 4 a set of characteristic functions, the $M_{2n}(x)$ functions, were defined and tabulated to allow the axial distributions of multipole strengths to be determined for a given body shape. (The problem of finding the body shape from the multipole distribution is a direct, although laborious, mathematical process.) The same characteristic functions are applicable to the particular set of multipoles used in reference 3. These multipoles written in several forms as follows

$$\frac{\cos 2n\theta \cosh\left(2n \cosh^{-1}\frac{x}{r}\right)}{\sqrt{x^2 - r^2}} = \frac{\cos 2n\theta}{2\sqrt{x^2-r^2}}\left[\left(\frac{x}{r} + \sqrt{\frac{x^2}{r^2} - 1}\right)^{n} + \left(\frac{x}{r} + \sqrt{\frac{x^2}{r^2} - 1}\right)^{-n}\right]$$

$$= \cos 2n\theta L^{-1}[K_{2n}(rs)] \tag{B1}$$

are distributed along the axis in strength $A_{2n}(x)$. The multipoles are started along the body axis at $x = 0$, as shown in sketch (j) so that

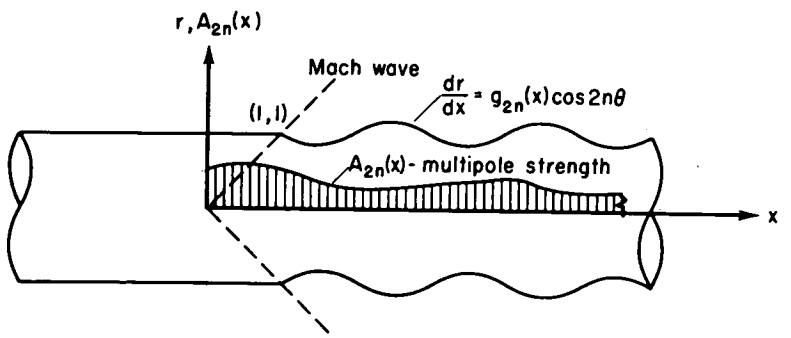

Sketch (j)

[redacted]

the body distortion starts at $x = 1$ for $M = \sqrt{2}$. The multipoles are not started at negative values of x since $A_{2n}(x)$ would not then have a Laplace transform when $x < 0$. The Laplace transform of the potential due to the multipoles is

$$\bar{\varphi}_M(s,r,\theta) = -\frac{1}{2\pi}\sum_{n=0}^{\infty}\bar{A}_{2n}(s)K_{2n}(sr)\cos 2n\theta \tag{B2}$$

and the potential in the physical space is

$$\varphi_M(x,r,\theta) = -\frac{1}{2\pi}\sum_{n=0}^{\infty}(\cos 2n\theta)\int_0^x A_{2n}(\xi)\frac{\cosh\left(2n\cosh^{-1}\frac{x-\xi}{r}\right)}{\sqrt{(x-\xi)^2-r^2}}\,d\xi \tag{B3}$$

Let φ_M be equal to φ_B produced by a distortion of the body given by equation (A1). Then, according to equation (A2) we have

$$\varphi_M(x,r,\theta) = \varphi_B(x,r,\theta) = V\left(\frac{t_m}{c_r}\right)L^{-1}\sum_{n=0}^{\infty}\frac{G_{2n}(s)K_{2n}(sr)}{sK_{2n}'(s)}\cos 2n\theta \tag{B4}$$

Comparison of equations (B2) and (B4) establishes the relationship between body shape and multipole strengths in the Laplace space as

$$G_{2n}(s) = -\frac{1}{2\pi V(t_m/c_r)}sK_{2n}'(s)\bar{A}_{2n}(s) \tag{B5}$$

Form the Faltung integral corresponding to equation (B5) with the help of the relation

$$L^{-1}\left[\frac{K_{2n}'(s)}{s}\right] = L^{-1}\left[K_{2n}(s)\right] = \frac{\cosh(2n \cosh^{-1}x)}{\sqrt{x^2-1}}; \quad x > 1$$

$$= 0; \quad x < 1$$

Thus

$$g_{2n}(x) = -\frac{1}{2\pi V(t_m/c_r)} \int_1^x A_{2n}''(\xi) \frac{\cosh(2n \cosh^{-1}x - \xi)}{\sqrt{(x-\xi)^2-1}} d\xi$$

$$= -\frac{1}{2\pi V(t_m/c_r)} \int_0^{x-1} A_{2n}''(\xi - 1) \frac{\cosh(2n \cosh^{-1}x - \xi + 1)}{\sqrt{(x-\xi+1)^2-1}} d\xi \tag{B6}$$

Equation (B6) gives a method of determining the shape of a quasi-cylinder corresponding to a given distribution of multipoles along the axis. The reverse problem of determining the multipole distributions for a given body shape is not as simple. This problem will arise whenever a minimum-drag wing-body combination is operated away from the design point. Equation (B5) is written in a form to facilitate the solution of the reverse problem

$$e^{-s} \bar{A}_{2n}(s) = -2\pi V\left(\frac{t_m}{c_r}\right) \frac{G_{2n}(s)}{se^s K_{2n}'(s)} \tag{B7}$$

The occurrence of $K_{2n}'(s)$ in the denominator makes the determination of the inverse transform difficult if at all possible in terms of known functions since the zeros of $K_{2n}'(s)$ in the complex plane are generally unknown. However, if we define the following function by its Laplace transform,

$$M_{2n}(x) \equiv L^{-1}\left[\frac{1}{se^s K_{2n}'(s)}\right] \tag{B8}$$

[redacted]

then the solution to the reverse problem can be written down

$$A_{2n}(x-1) = -2\pi V\left(\frac{t_m}{cr}\right)\int_1^x g_{2n}(\xi)M_{2n}(x-\xi)d\xi \qquad (B9)$$

Tabulated values of $M_0(x)$, $M_2(x)$, $M_4(x)$, and $M_6(x)$ for $0 \leq x \leq 4$ are included in reference 5 for numerical work. Equation (B9) thus allows a simple calculation of the multipole strengths for a given shape. The functions $M_{2n}(x)$ have logarithmic singularities at the origin. Thus whenever $g_{2n}(x)$ is finite, so is $A_{2n}(x-1)$, and if $g_{2n}(x)$ has a singularity, so will $A_{2n}(x-1)$.

APPENDIX C

ALTERNATE METHOD FOR DETERMINING BODY SHAPE FOR MINIMUM-DRAG COMBINATION

In this appendix we will consider the solution for the body shape for minimum drag by the method of reference 3, and its relationship to the present method. In reference 3, the potential function for a general class of minimum-drag combinations is found without recourse to solving a boundary-value problem as already described in the Introduction. If the stream tubes corresponding to the potential are known, any stream tube can be replaced by a body to form a minimum-drag wing-body combination. To carry out the precise determination of the body shape requires the simultaneous solution of a pair of nonlinear differential equations. Practically, the shape must be calculated by some approximate method. However, the potential function for the minimum-drag combination is accurate to the order of linear theory. In the quasi-cylindrical theory it is assumed that the flow is known for a cylindrical body and wing combination by the use of the interference methods of references 4, 5, and 6. Then the shape perturbation from the circular cylinder necessary to produce minimum drag is calculated harmonic by harmonic. In this method the boundary conditions are applied on the $r = 1$ cylinder. The potential for the minimum-drag combination will not be mathematically identical to that given by the multipole solution because the body boundary conditions in the quasi-cylindrical problem have not been applied precisely on the body. (For both solutions the wing boundary conditions are applied on the $z = 0$ plane instead of on the wing surface.) However, for thin enough wing panels the minimum-drag body will approach a cylindrical body as closely as desired. Under these conditions we may therefore equate the potentials given by the two methods to the order of linear theory.

In the present paper, the combination potential is

$$\varphi_C = \varphi_W + \varphi_i + \varphi_B \tag{C1}$$

and in reference 3 the combination potential is

$$\varphi_C = \varphi_W + \varphi_M \tag{C2}$$

where φ_M is the potential due to the canceling multipoles. We can thus say that to the order of linear theory

$$\varphi_i + \varphi_B = \varphi_M \tag{C3}$$

Since from equations (B2) and (A4) the following relationships are true,

$$L(\varphi_M) = -\frac{1}{2\pi}\sum_{n=0}^{\infty} \cos 2n\theta\ \bar{A}_{2n}(s)K_{2n}(sr)$$

$$L(\varphi_B) = V\left(\frac{t_m}{c_r}\right)\sum_{n=0}^{\infty} \cos 2n\theta\ \frac{G_{2n}(s)K_{2n}(sr)}{sK_{2n}'(s)}$$

$$L(\varphi_i) = V\left(\frac{t_m}{c_r}\right)\sum_{n=0}^{\infty} \cos 2n\theta\ \frac{F_{2n}(s)K_{2n}(sr)}{sK_{2n}'(s)}$$

we obtain the following relationship among the variables

$$G_{2n}(s) = -F_{2n}(s) - \frac{1}{2\pi V(t_m/c_r)}\bar{A}_{2n}(s)sK_{2n}'(s) \qquad (C4)$$

The following relationships permit us to form the Faltung integral corresponding to equation (C4).

$$L^{-1}\left[\frac{K_{2n}'(s)}{s}\right] = L^{-1}[K_{2n}(s)] = \frac{\cosh(2n\ \cosh^{-1}x)}{\sqrt{x^2-1}}; \qquad x > 1$$

$$= 0 \qquad ; \qquad x < 1 \qquad (C5)$$

The inverse of equation (C4) is thus

$$g_{2n}(x) = -f_{2n}(x) - \frac{1}{2\pi V(t_m/c_r)}\int_1^x A_{2n}''(\xi)\frac{\cosh[2n\ \cosh^{-1}(x-\xi)]}{\sqrt{(x-\xi)^2-1}}\,d\xi \qquad (C6)$$

The first term can be thought of as the virtual distortion of the cylinder by the wing-alone field, and the second term is the body distortion due

to the canceling multipoles. The multipole strengths are determined by the method of oblique planes as used in the supersonic area rule and described in references 3 and 8.

The value of the shape amplitude functions, $g_{2n}(x)$, can, in principle, be determined analytically from equation (C6). The determination involves first calculating the normal velocity field at the $r = 1$ cylinder due to the wing alone and performing a Fourier analysis to obtain the $f_{2n}(x)$ functions. Then the multipole strength distributions for the wing alone $A_{2n}(\xi)$ are obtained by the method of oblique cuts which includes a Fourier analysis. Finally, to obtain the shape amplitude functions, the integrals of equation (C6) must be evaluated.

APPENDIX D

PRANDTL-GLAUERT TRANSFORMATION FOR WING-BODY COMBINATION

The calculations for the example configuration have all been made for a Mach number of $\sqrt{2}$, but the results can be generalized to any Mach number by means of the Prandtl-Glauert rule. Let the configuration at Mach number M be transformed into an equivalent $M = \sqrt{2}$ configuration by dividing its longitudinal dimensions by β and leaving its lateral dimension unchanged. Let the potential at corresponding points be the same (see fig. 20). The two potential fields are solutions to the differential equations given in the figure. Since the potential is the same in the y and z dimensions, $\partial\varphi/\partial y$ and $\partial\varphi/\partial z$ are unaltered so that the slopes of all surfaces in the streamwise direction are unaltered. Under these conditions the quantities at M and at $M = \sqrt{2}$ are related as follows:

$$\left.\begin{aligned} c_{r_M} &= \beta c_{r_{\sqrt{2}}} \\ t_{m_M} &= \beta t_{m_{\sqrt{2}}} \\ s_M &= s_{\sqrt{2}} \\ V_{i_M} &= \beta^2 V_{i_{\sqrt{2}}} \\ V_{W_M} &= \beta^2 V_{W_{\sqrt{2}}} \\ D_M &= D_{\sqrt{2}} \end{aligned}\right\} \qquad (D1)$$

At corresponding points x,y,z at M and $x/\beta,y,z$ at $M = \sqrt{2}$ we have

$$\left.\begin{aligned} P_M &= \frac{1}{\beta} P_{\sqrt{2}} \\ \left(\frac{dr}{dx}\right)_M &= \left(\frac{dr}{dx}\right)_{\sqrt{2}} ; \qquad r = 1 \\ \left(\frac{dz_u}{dx}\right)_M &= \left(\frac{dz_u}{dx}\right)_{\sqrt{2}} ; \qquad \theta = 0,\pi \end{aligned}\right\} \qquad (D2)$$

[redacted]

The calculated results at $M = \sqrt{2}$ can be generalized to apply to all combinations of the family - in our case all combinations with sonic edges and fixed body radius and combination span - by plotting $\frac{1-(r_B/a)}{\beta(t_m/c)}$ versus $x/\beta a$ for body indentations, $\beta P/(t_m/c)$ versus $x/\beta a$ with r/a as parameter for wing pressure distributions, $\beta C_D/(t_m/c)^2$ versus s/a or βA_E with $c/\beta a$ as parameter for drag, and Vi/V_W versus s/a or βA_E with $c/\beta a$ as parameter for volume of cut-out.

REFERENCES

1. Whitcomb, Richard T.: A Study of the Zero-Lift Drag-Rise Characteristics of Wing-Body Combinations Near the Speed of Sound. NACA RM L52H08, 1952.

2. Hayes, W. D.: Linearized Supersonic Flow. Doctoral Thesis, Calif. Inst. of Tech., Pasadena, Calif., 1947.

3. Lomax, H., and Heaslet, M.: A Special Method for Finding Body Distortions that Reduce the Wave Drag of Wing and Body Combinations at Supersonic Speeds. NACA RM A55B16, 1955.

4. Nielsen, Jack N.: Supersonic Wing-Body Interference. Doctoral Thesis, Calif. Inst. of Tech., Pasadena, Calif., 1951.

5. Nielsen, Jack N., and Pitts, William C.: Wing-Body Interference at Supersonic Speeds With an Application to Combinations With Rectangular Wings. NACA TN 2677, 1952.

6. Pitts, William C., Nielsen, Jack N., and Gionfriddo, Maurice P.: Comparison Between Theory and Experiment for Interference Pressure Field Between Wing and Body at Supersonic Speeds. NACA TN 3128, 1954.

7. Jones, Robert T.: Thin Oblique Airfoils at Supersonic Speed. NACA TN 1107, 1946.

8. Jones, Robert T.: Theory of Wing-Body Drag at Supersonic Speeds. NACA RM A53H18a, 1953.

9. Whitcomb, Richard T., and Fischetti, Thomas L.: Development of a Supersonic Area Rule and an Application to the Design of a Wing-Body Combination Having High Lift-to-Drag Ratios. NACA RM L53H31a, 1953.

10. Nielsen, Jack N., and Matteson, Frederick H.: Calculative Method for Estimating the Interference Pressure Field at Zero Lift on a Symmetrical Swept-Back Wing Mounted on a Circular Cylindrical Body. NACA RM A9E19, 1949.

11. Bogdonoff, S. M., and Kepler, C. E.: Separation of a Supersonic Turbulent Boundary Layer. Office of Naval Research Rep. No. 249, Jan. 1954.

[redacted]

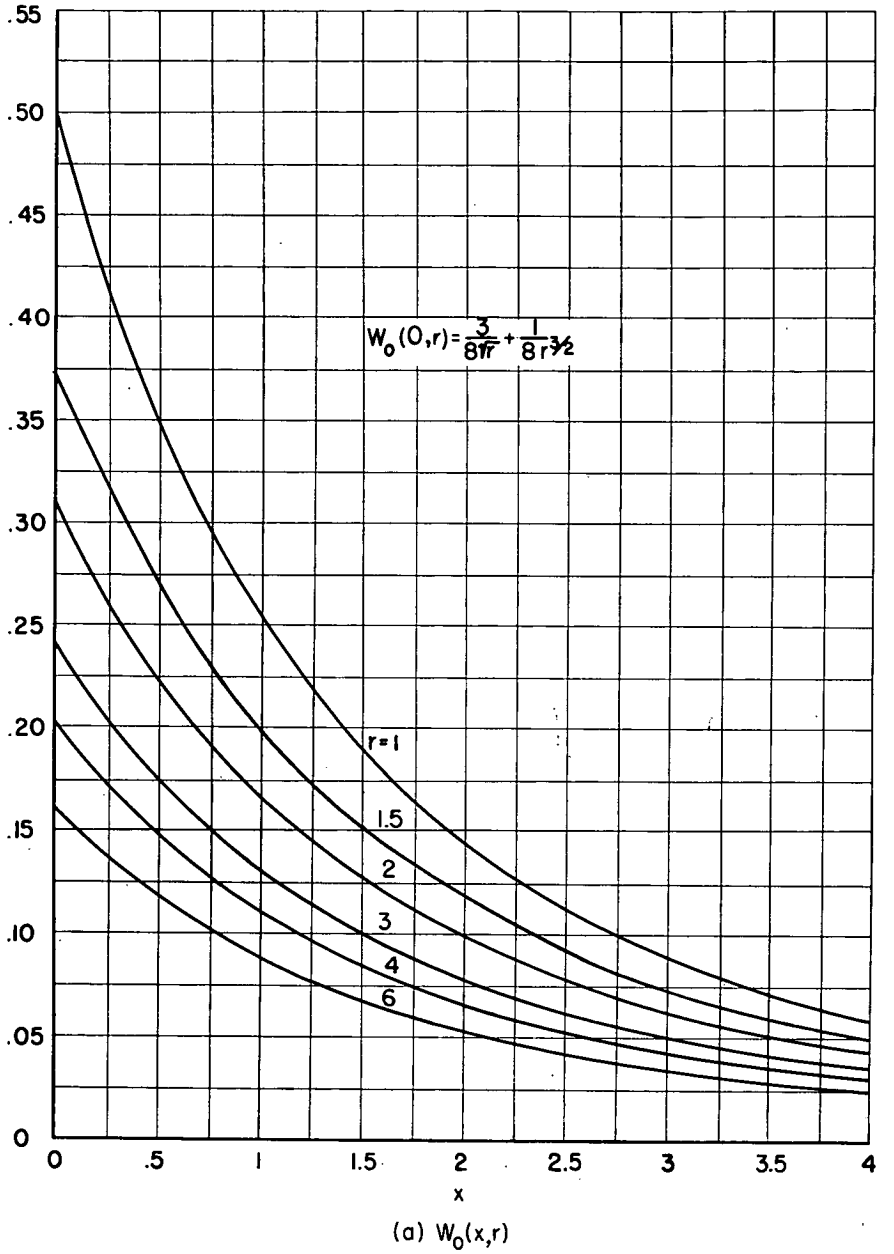

Figure 1.- Charts of characteristic functions.

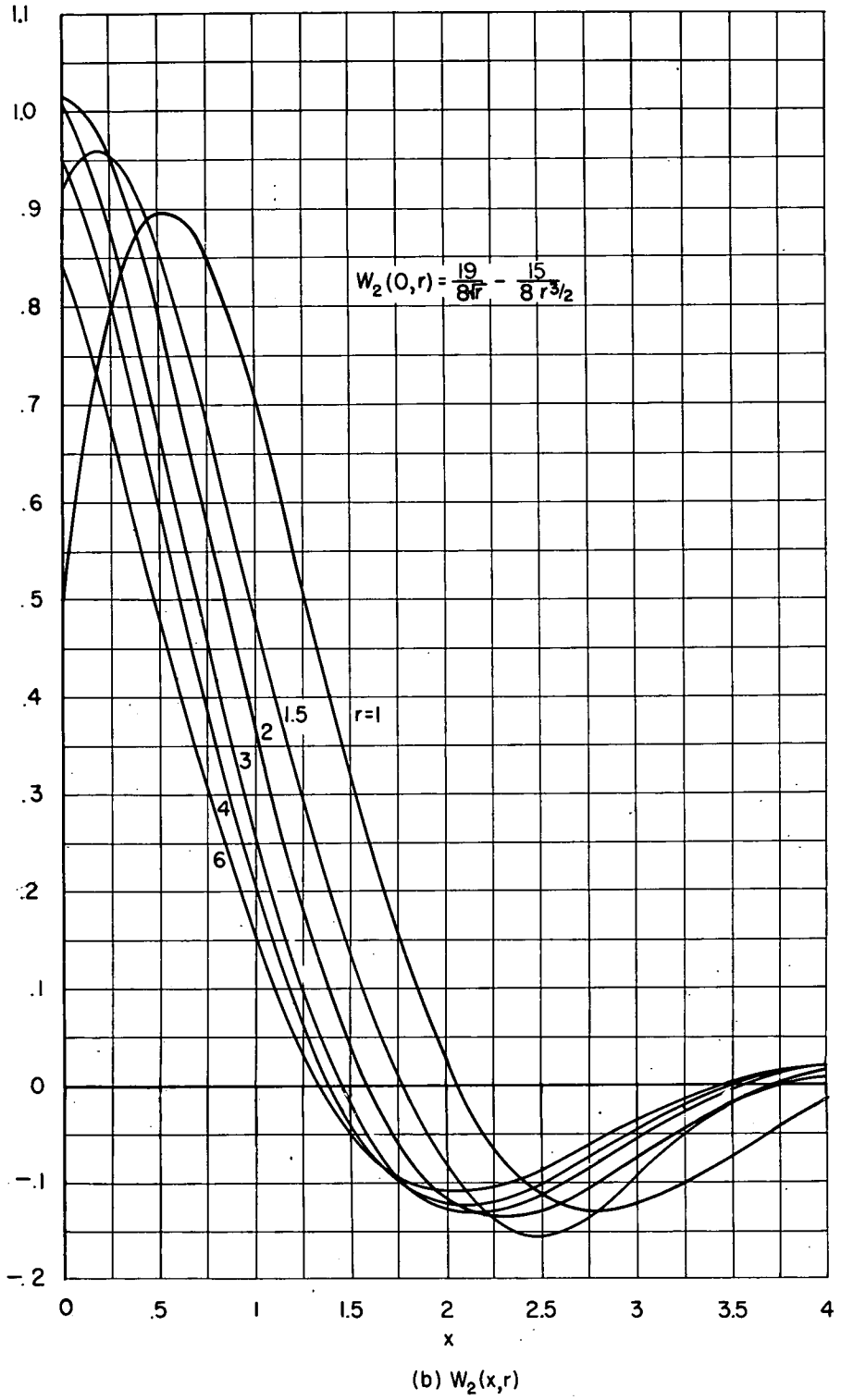

(b) $W_2(x,r)$

Figure 1.- Concluded.

[redacted]

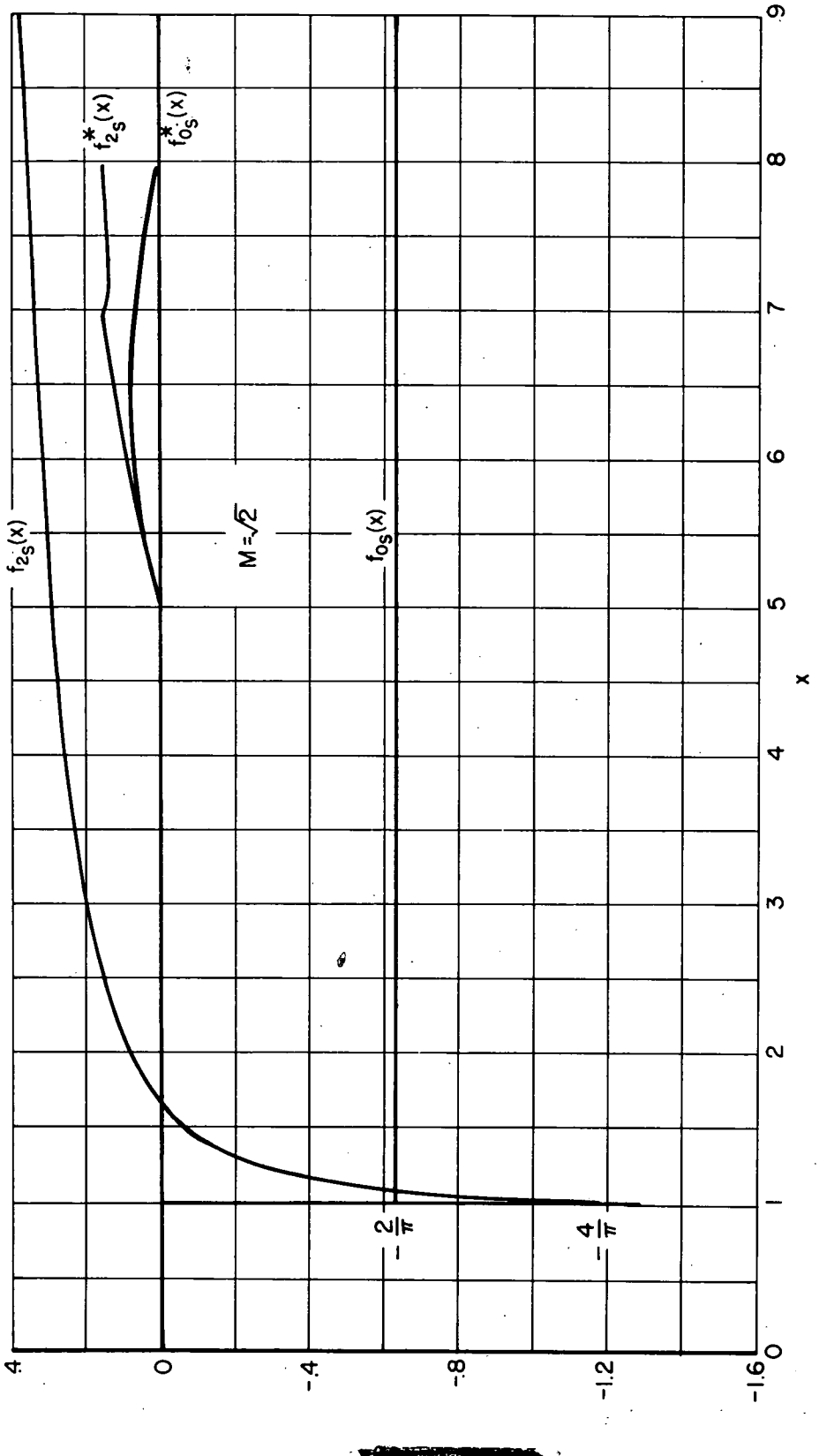

Figure 2.- Velocity amplitude functions for source pairs.

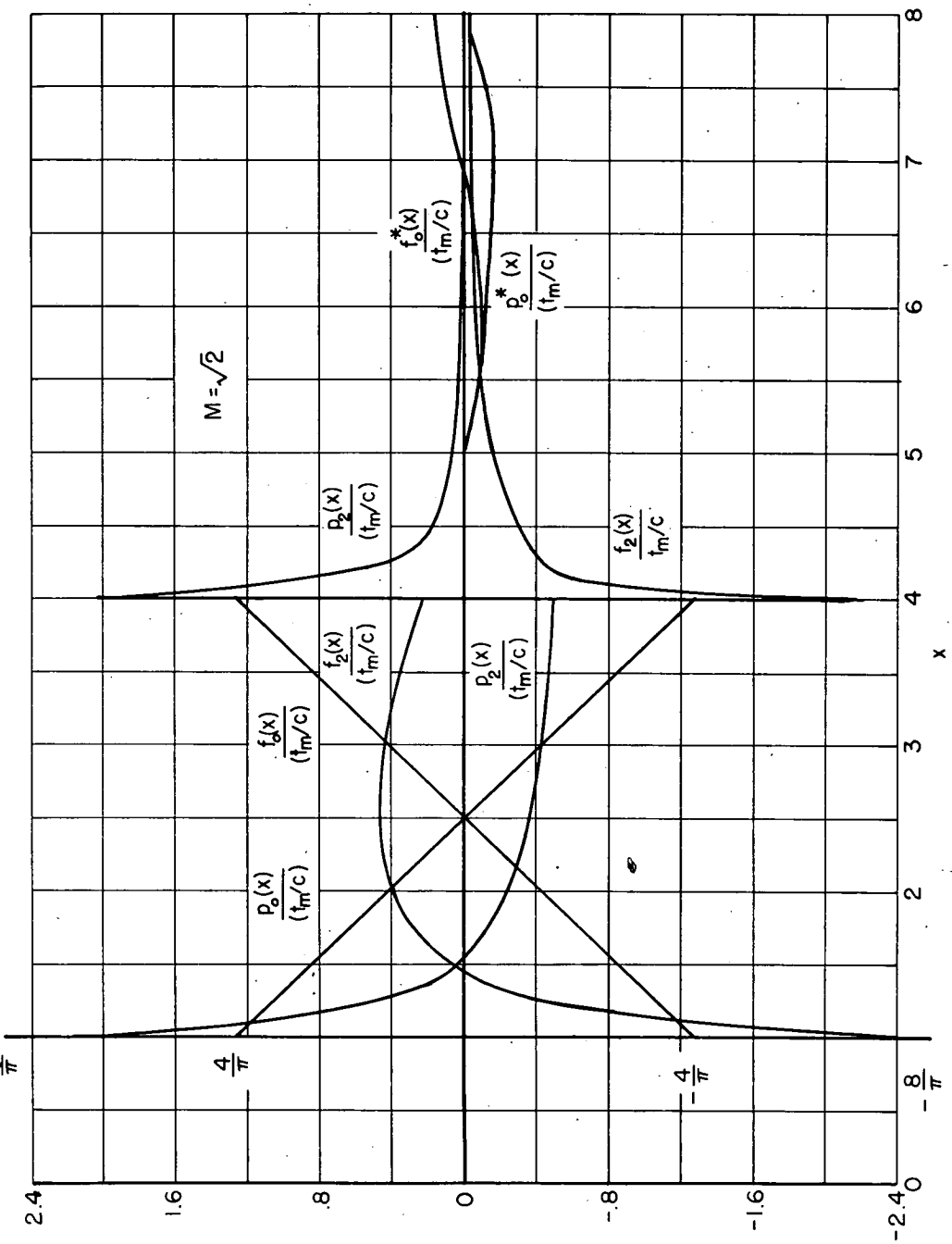

Figure 3.- Velocity and pressure amplitude functions for wing alone.

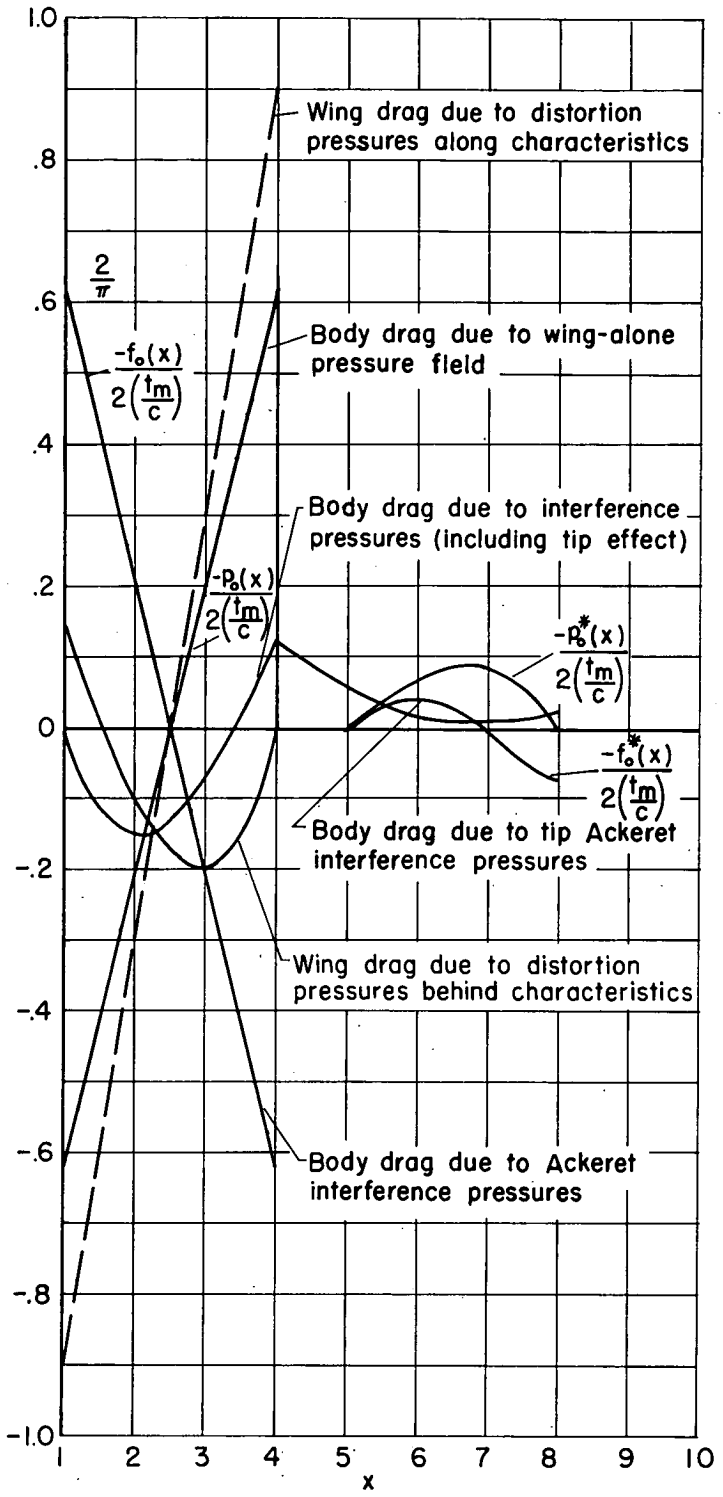

Figure 4.- Components of $h_o(x)$.

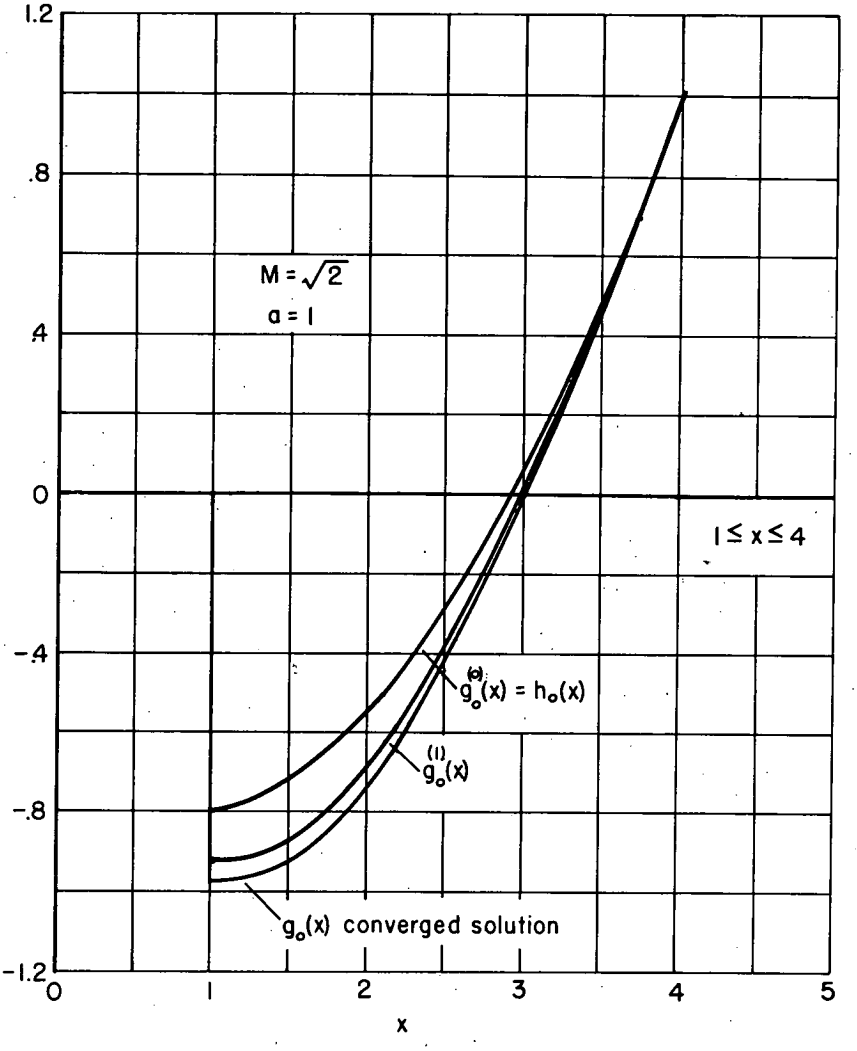

Figure 5.- Successive approximations in solution to integral equation for $n = 0$.

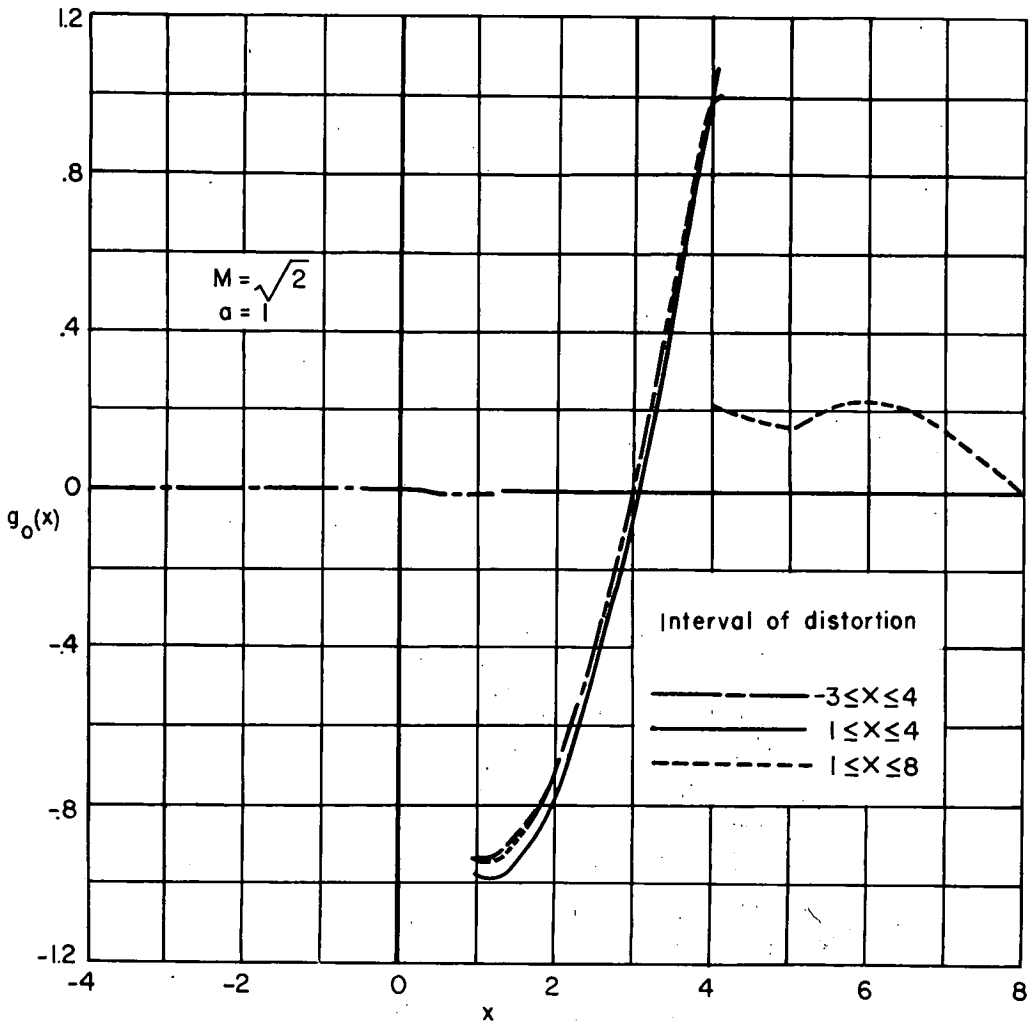

Figure 6.- Dependence of $g_0(x)$ on interval of distortion.

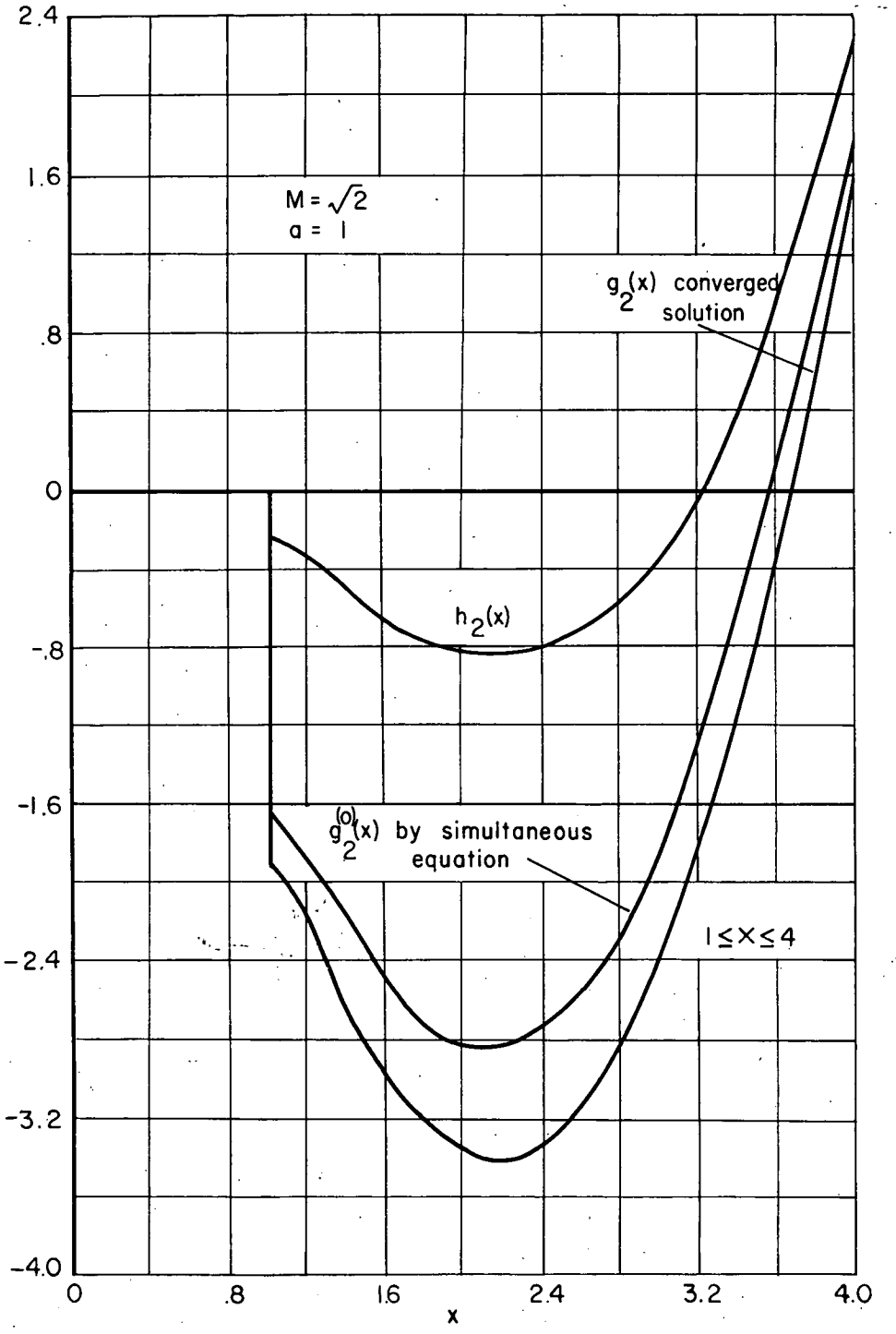

Figure 7.- Successive approximations in solution to integral equation for n = 1.

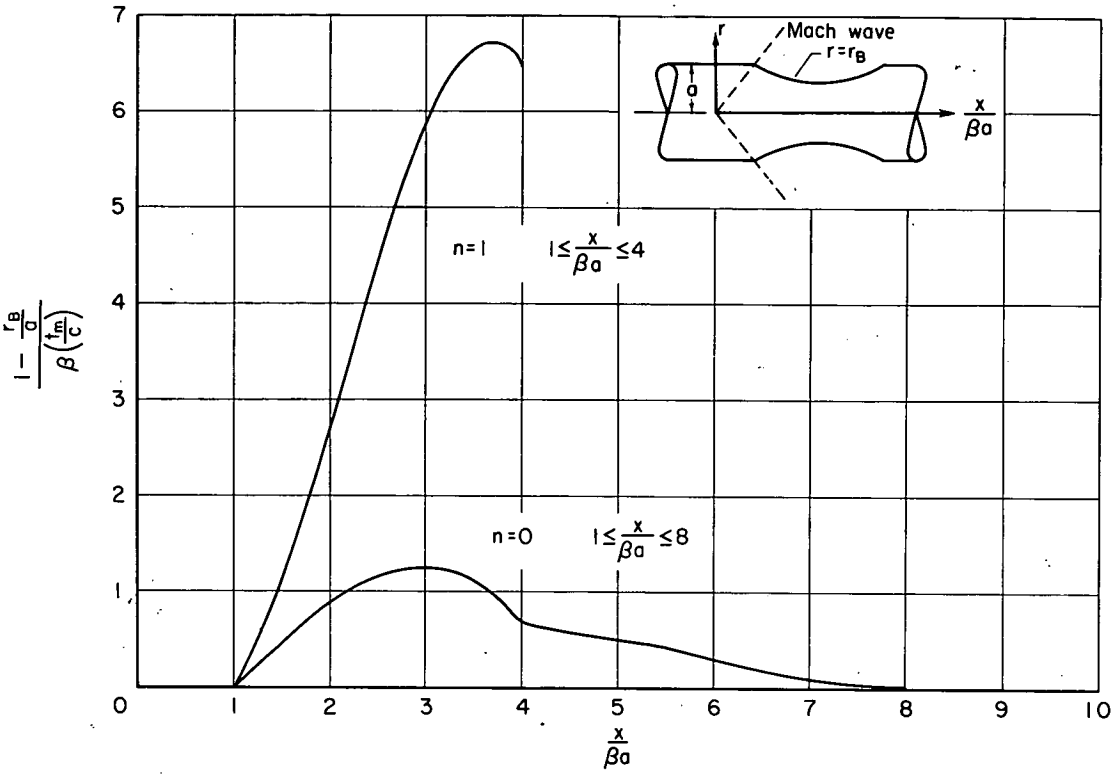

Figure 8.- Contribution of axially symmetric and second harmonics to body indentation at wing juncture.

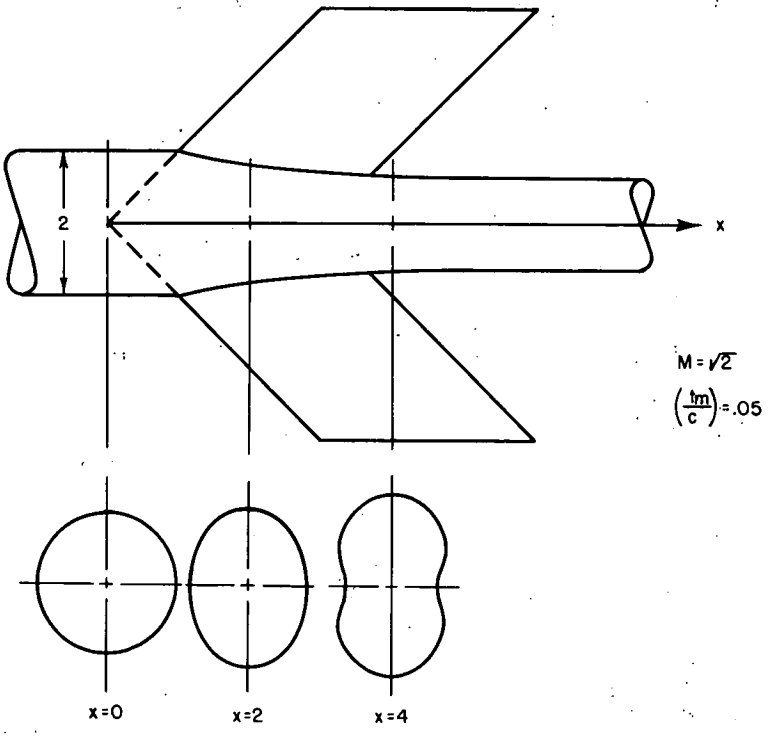

Figure 9.- Shape of distorted body.

CONFIDENTIAL

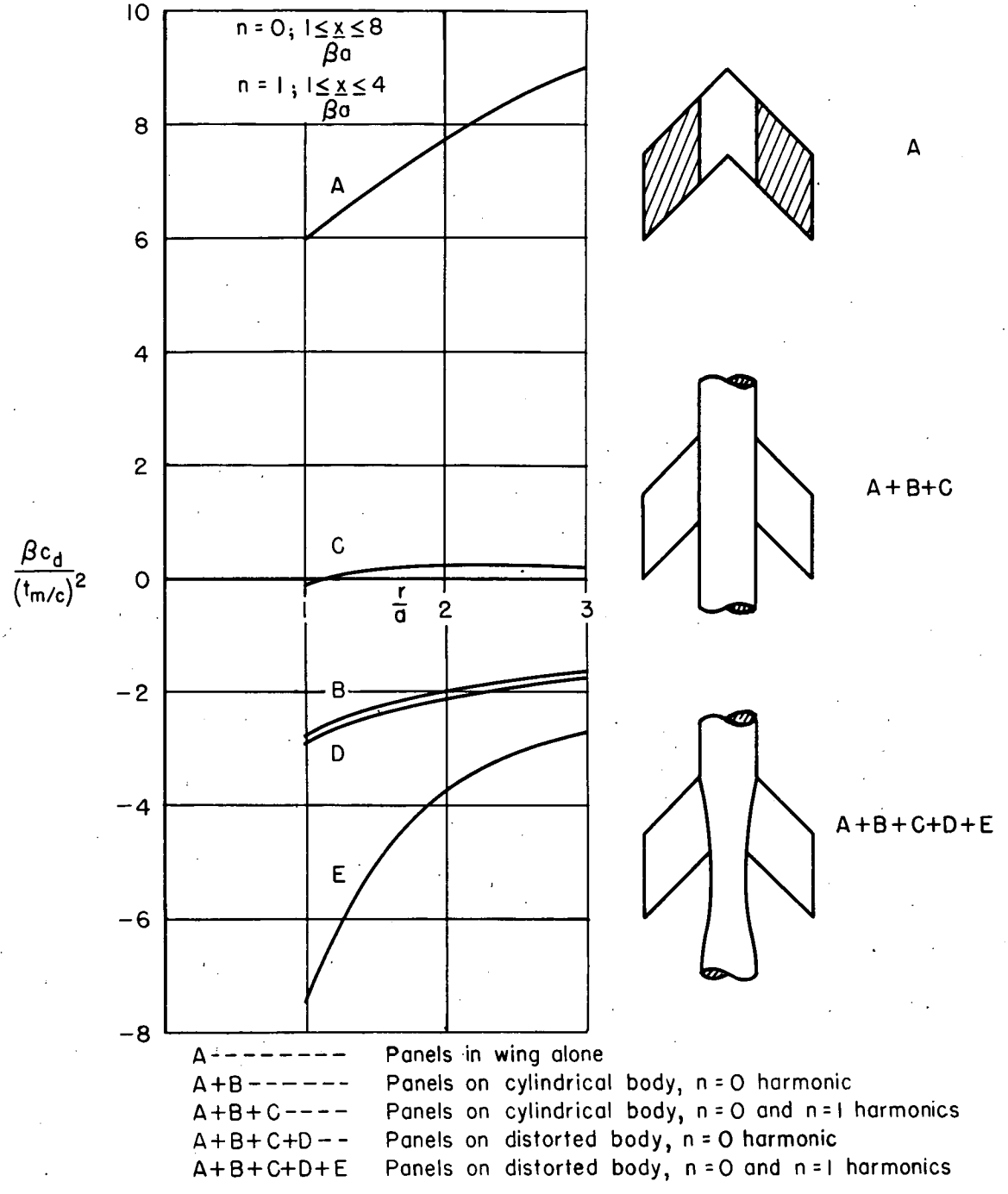

Figure 10.- Spanwise distribution of drag on wing panels in combination with various bodies.

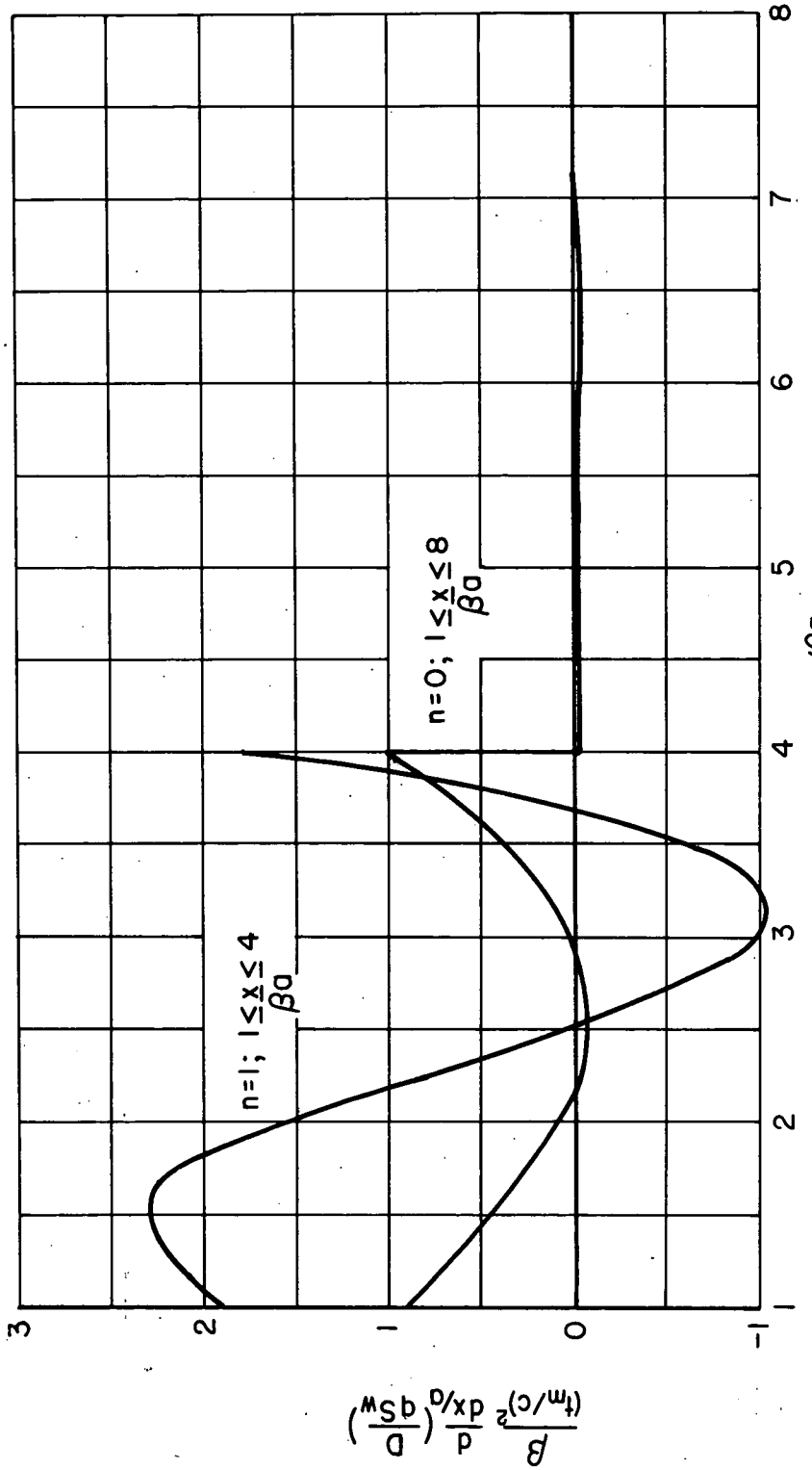

Figure 11.- Drag loading along body due to n = 0 and n = 1 harmonics of distortion.

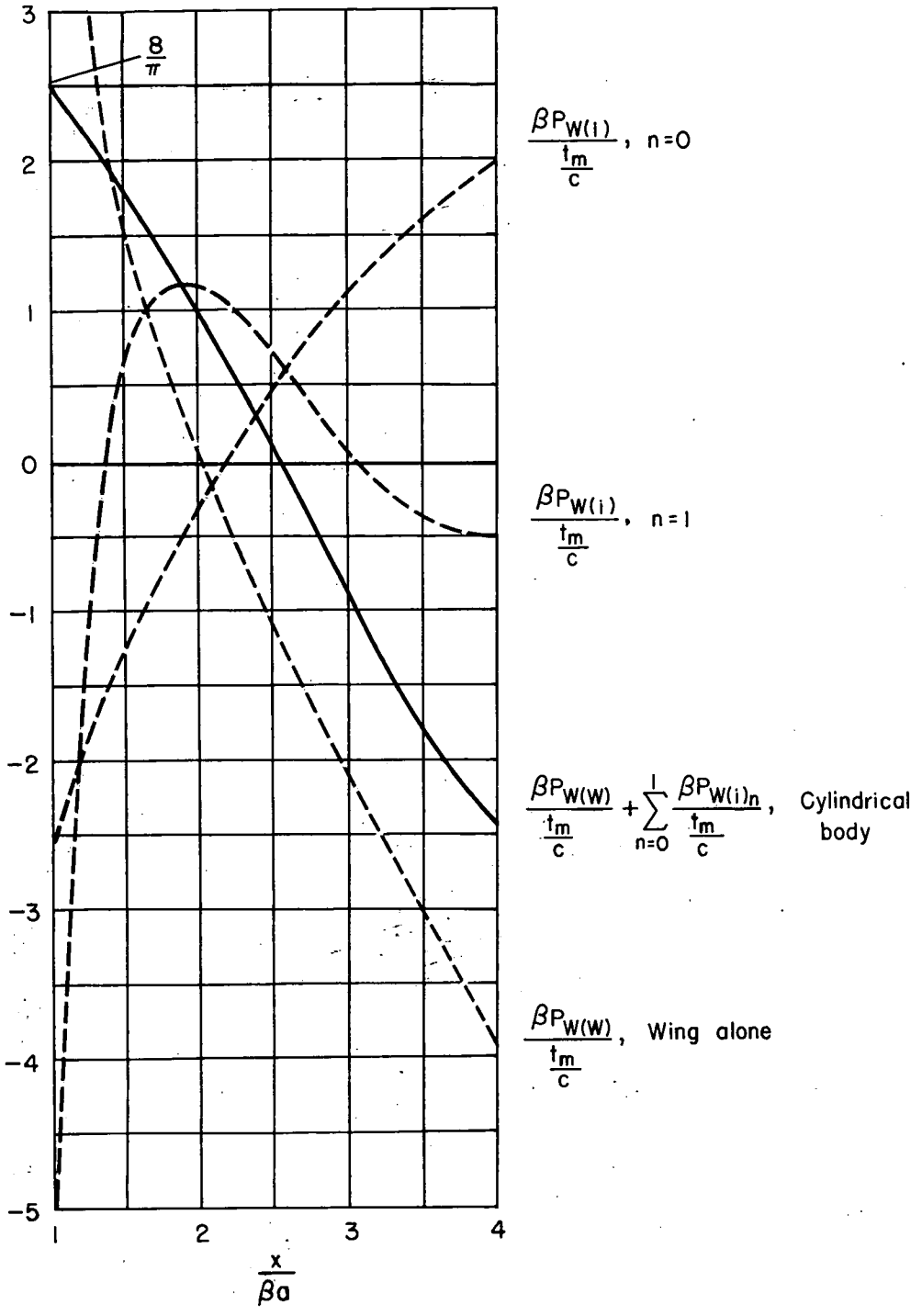

(a) Cylindrical body.

Figure 12.- Pressure distribution at wing-body juncture.

[redacted]

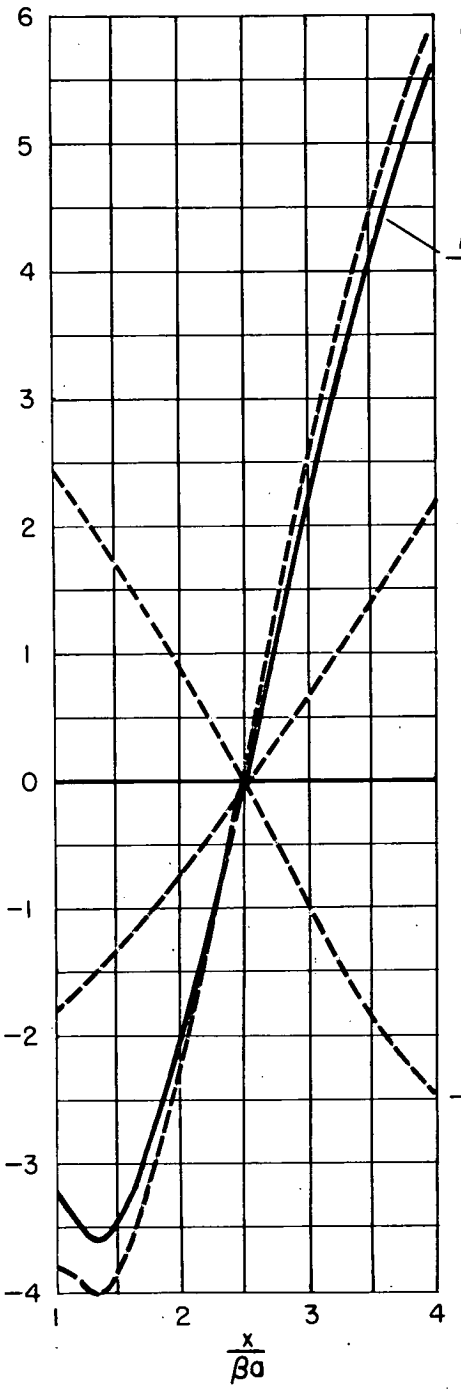

$\frac{\beta P_{W(d)}}{t_m/c}, n=1 \quad 1 \le \frac{x}{\beta a} \le 4$

$\frac{\beta P_{W(W)}}{(t_m/c)} + \sum_{n=0}^{1}\left[\frac{\beta P_{W(i)_n}}{(t_m/c)} + \frac{\beta P_{W(d)_n}}{(t_m/c)}\right]$, Distorted body

$\frac{\beta P_{W(d)}}{t_m/c}, n=0 \quad 1 \le \frac{x}{\beta a} \le 8$

$\frac{\beta P_{W(W)}}{(t_m/c)} + \sum_{n=0}^{1} \frac{\beta P_{W(i)_n}}{(t_m/c)}$, Cylindrical body

(b) Distorted body.

Figure 12.- Concluded.

[redacted]

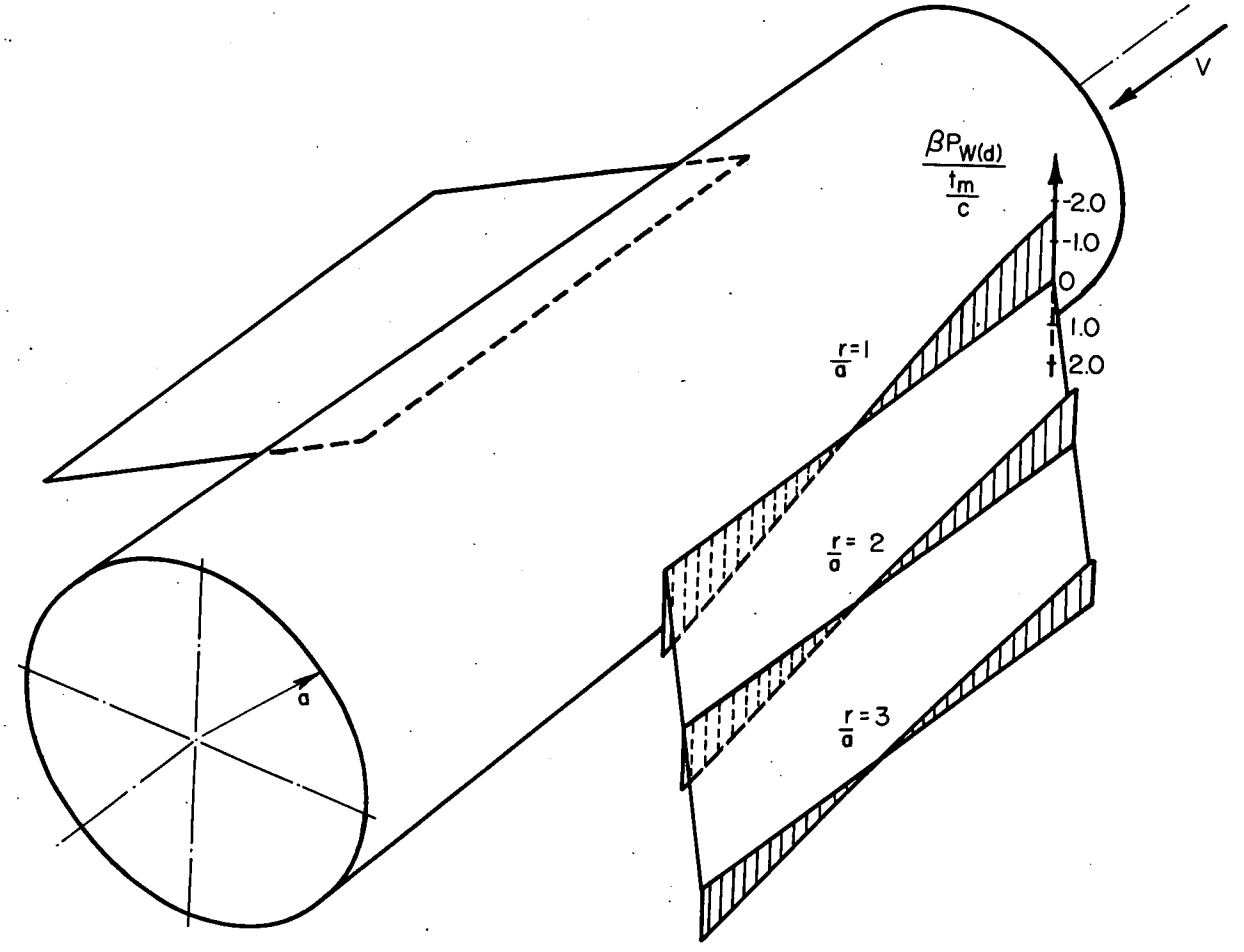

(a) Axially symmetric harmonic.

Figure 13.- Spanwise attenuation of wing pressure coefficients due to body distortion.

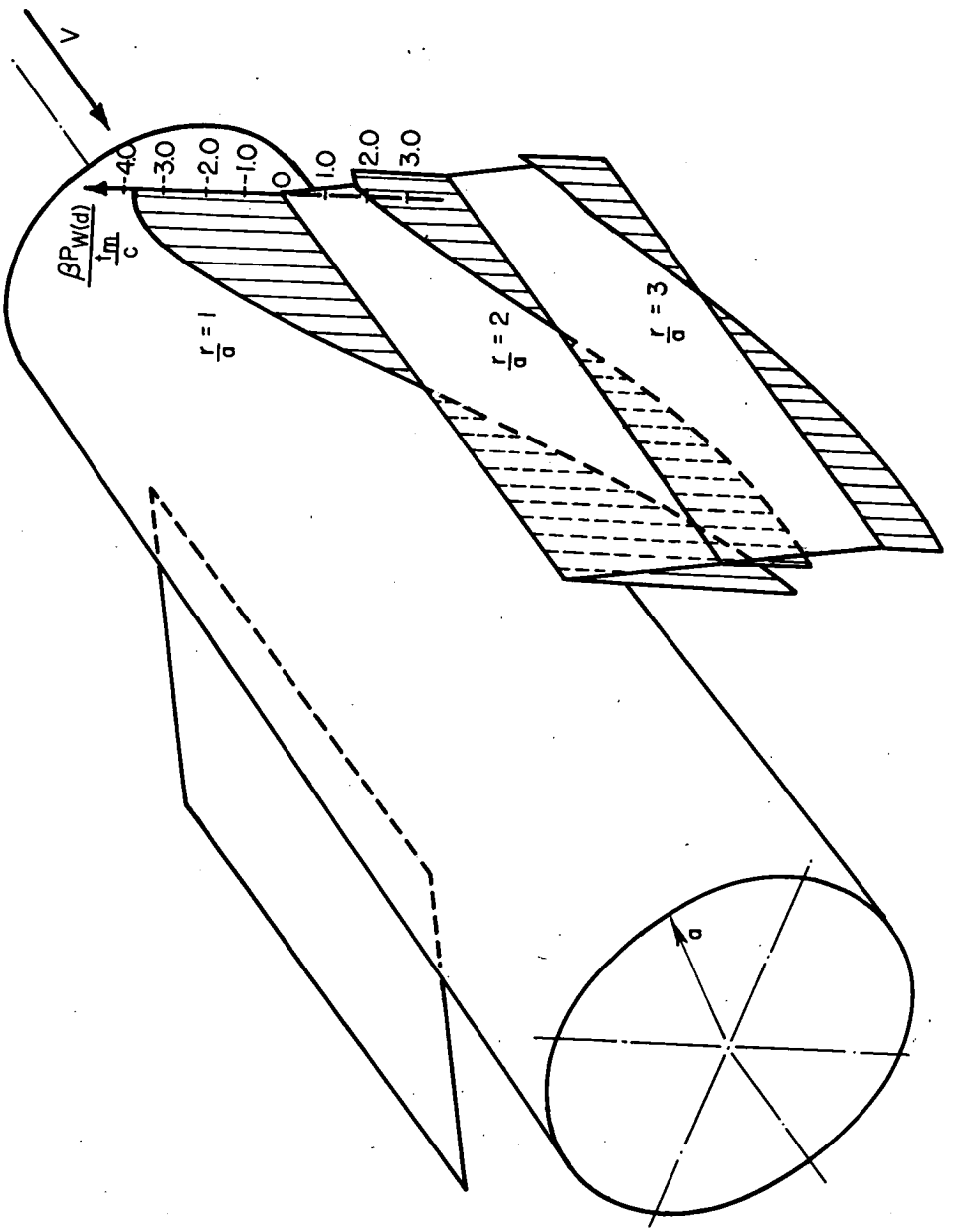

(b) Second harmonic.

Figure 13.- Concluded.

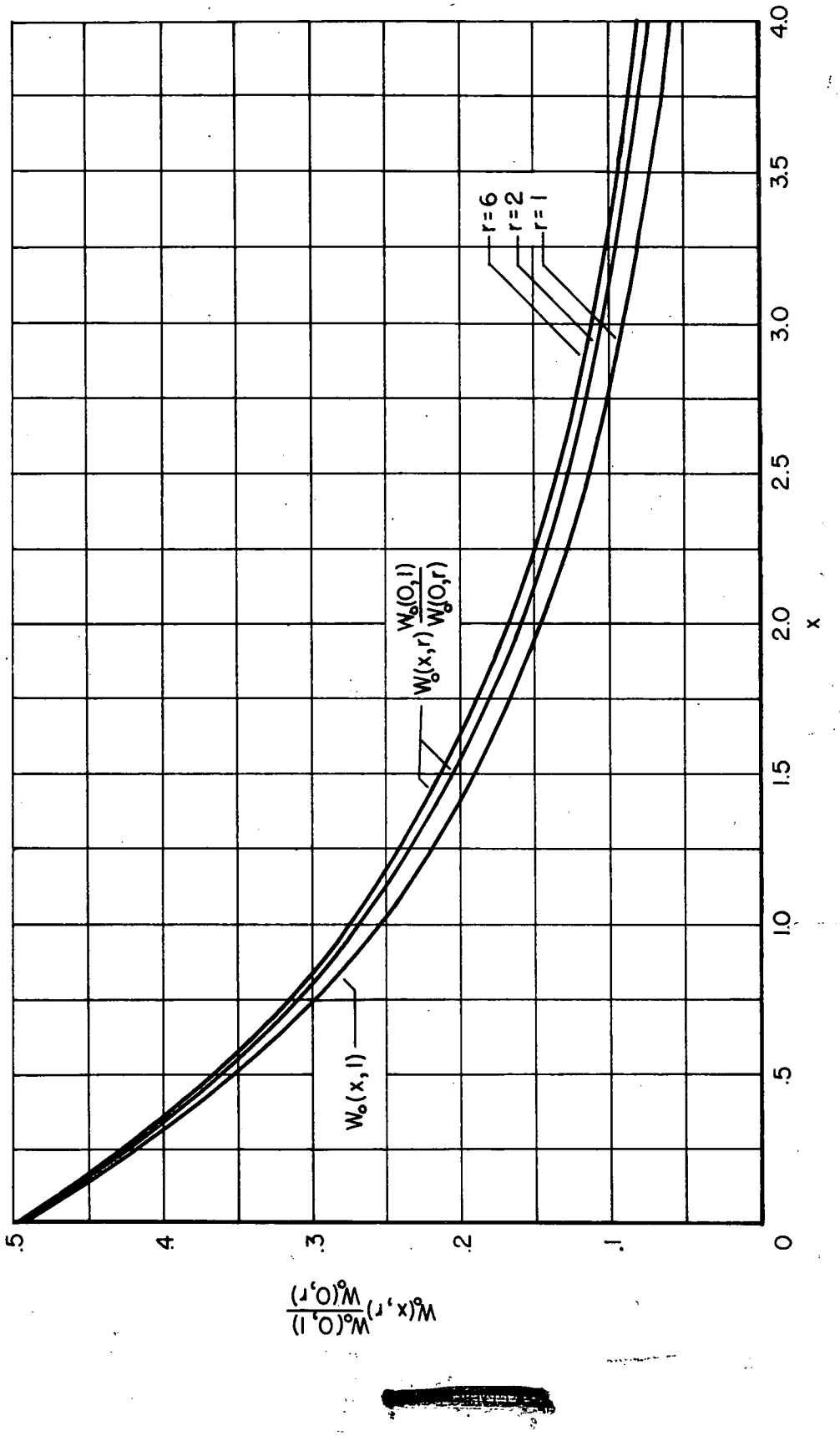

Figure 14.- Variation of $W_o(x,r)\ W_o(0,1)/W_o(0,r)$ with radius.

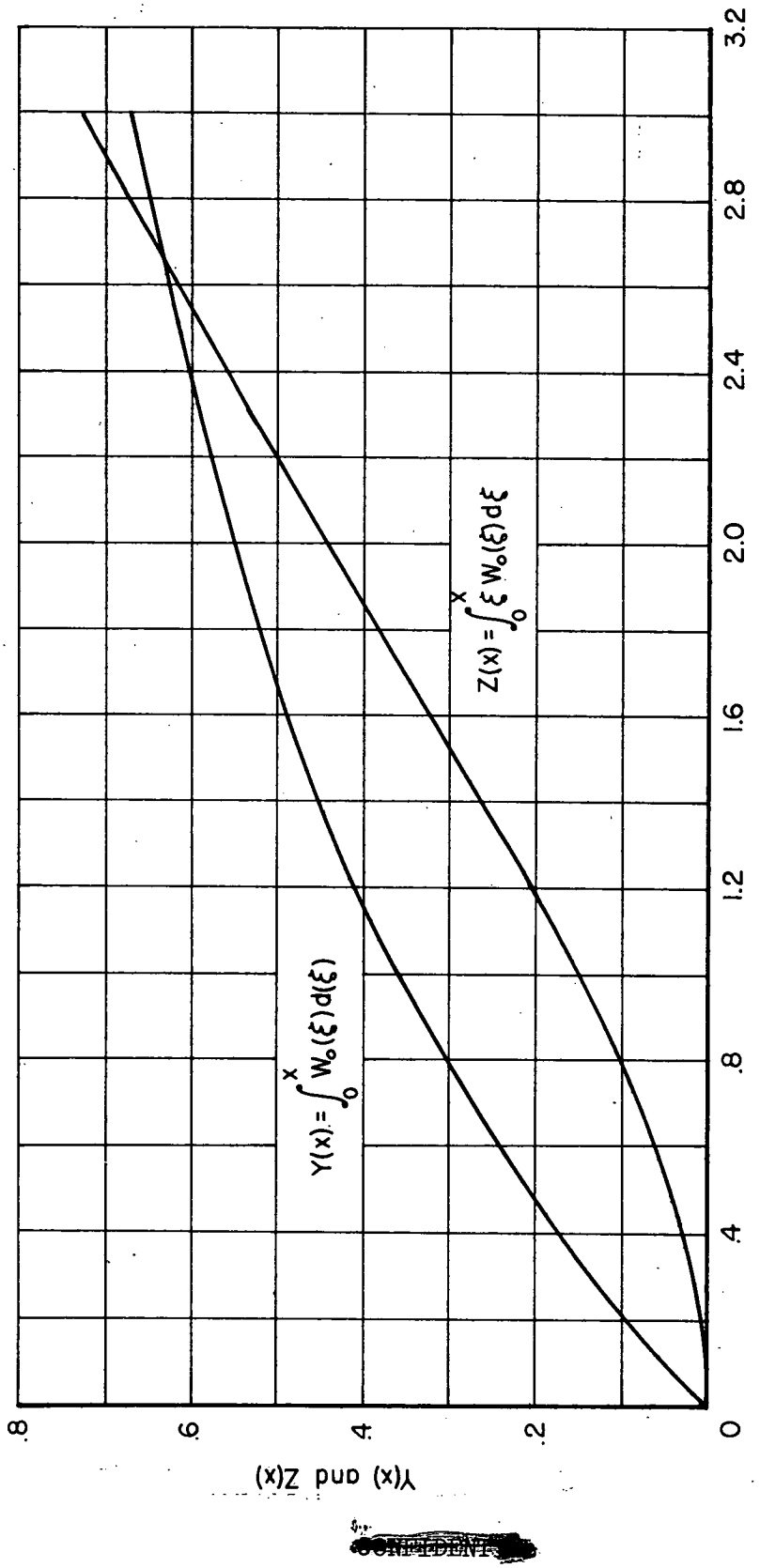

Figure 15.- Values of Y(x) and Z(x).

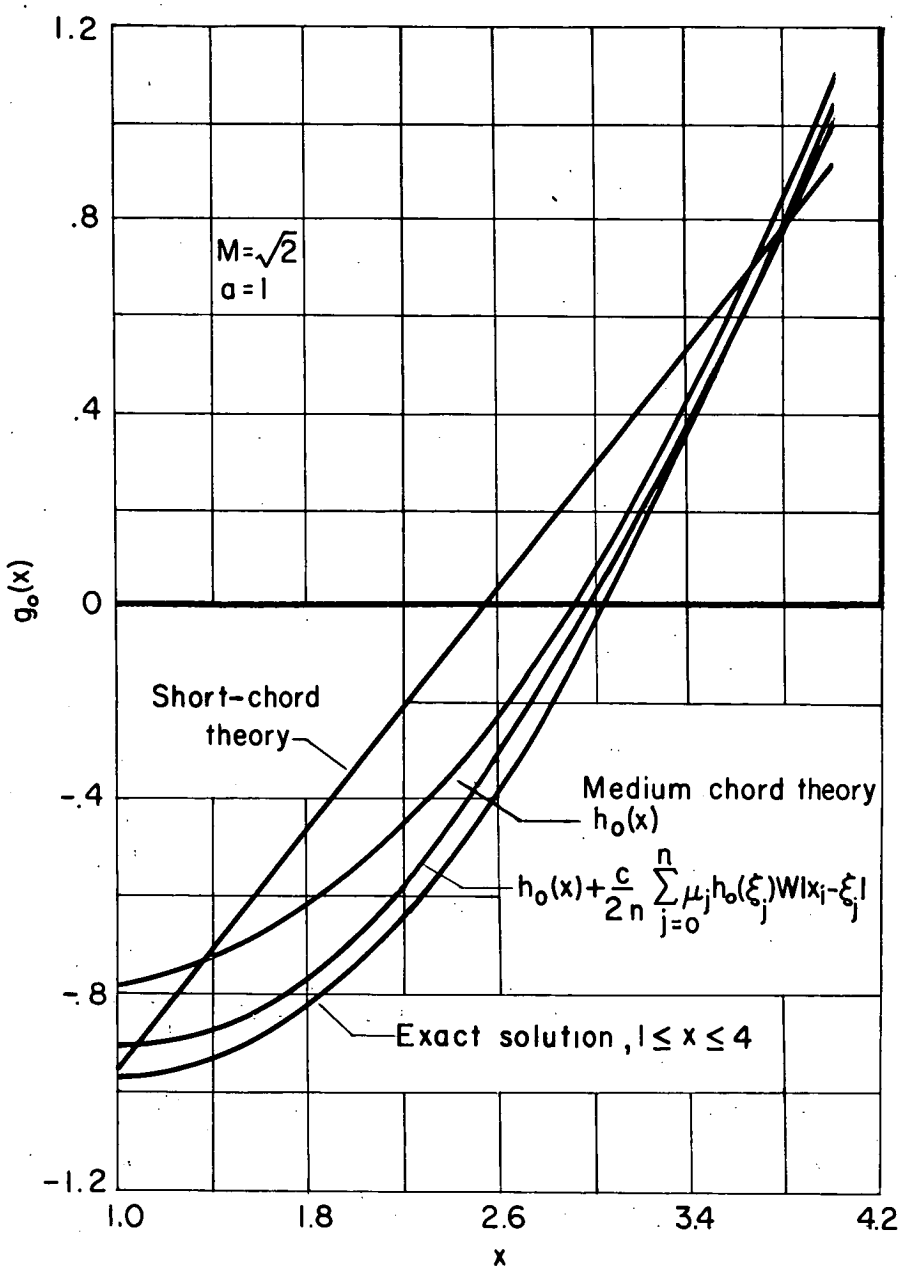

Figure 16.- Comparison of indentation by approximate and exact theories.

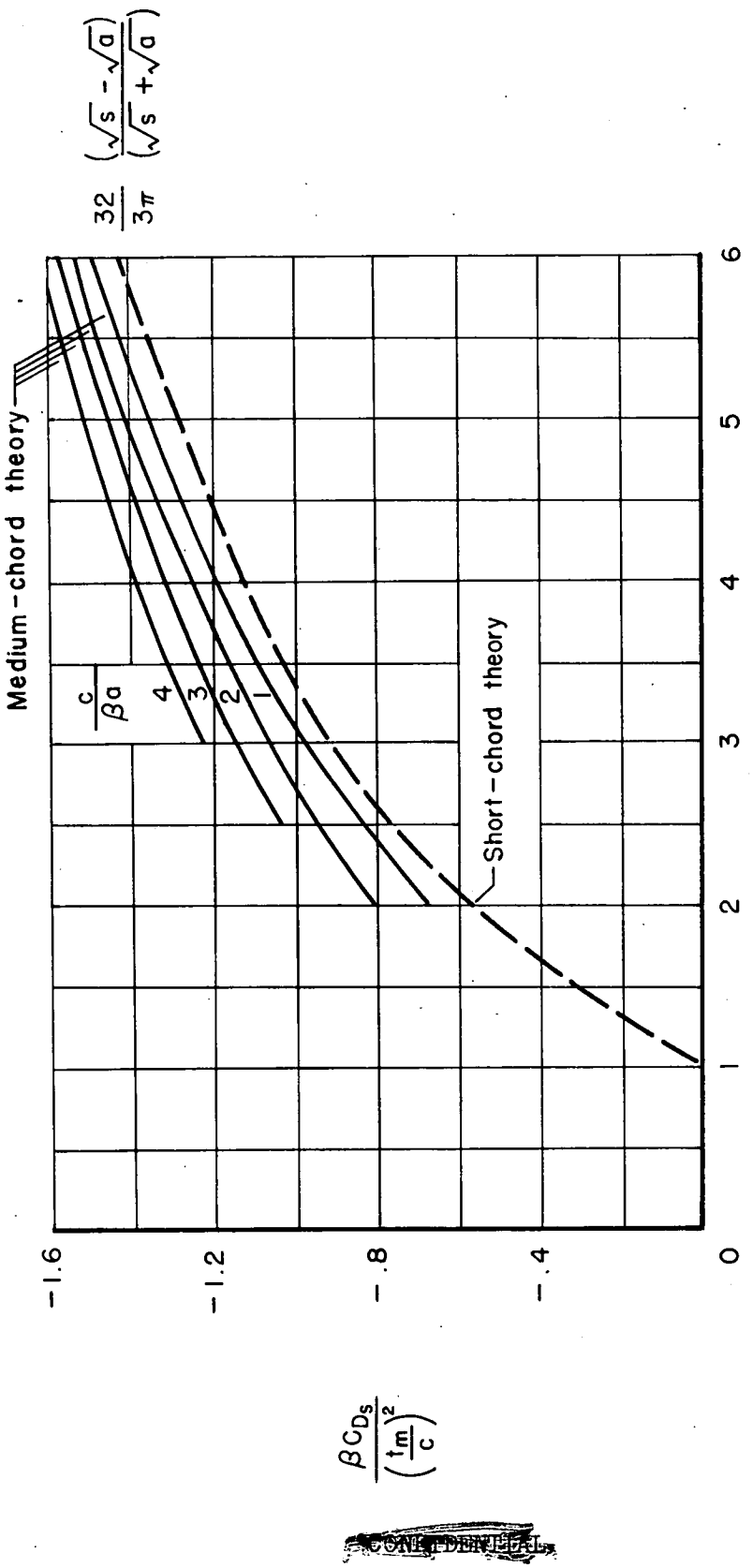

Figure 17.- Effect of span and chord on coefficient of drag saving for n = 0 harmonic.

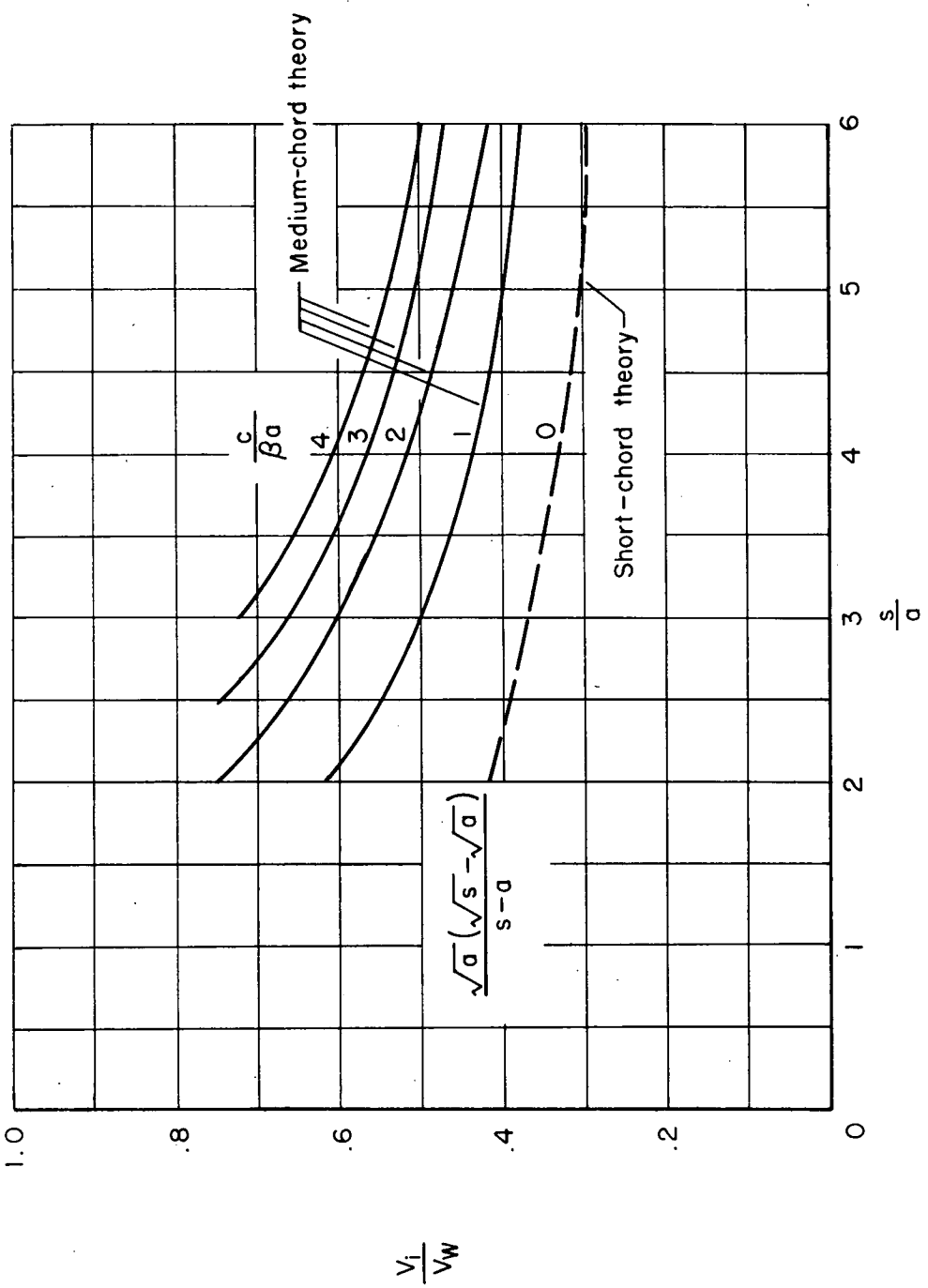

Figure 18.- Effect of span and chord on volume of indentation for n = 0 harmonic as fraction of wing volume.

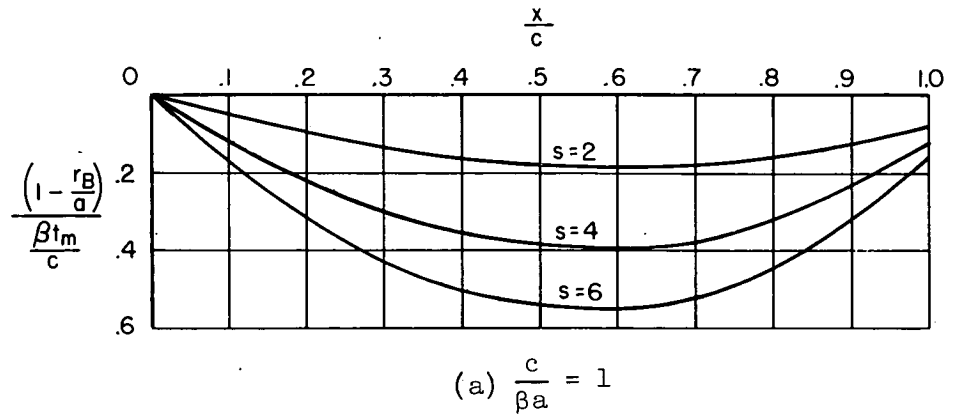

(a) $\frac{c}{\beta a} = 1$

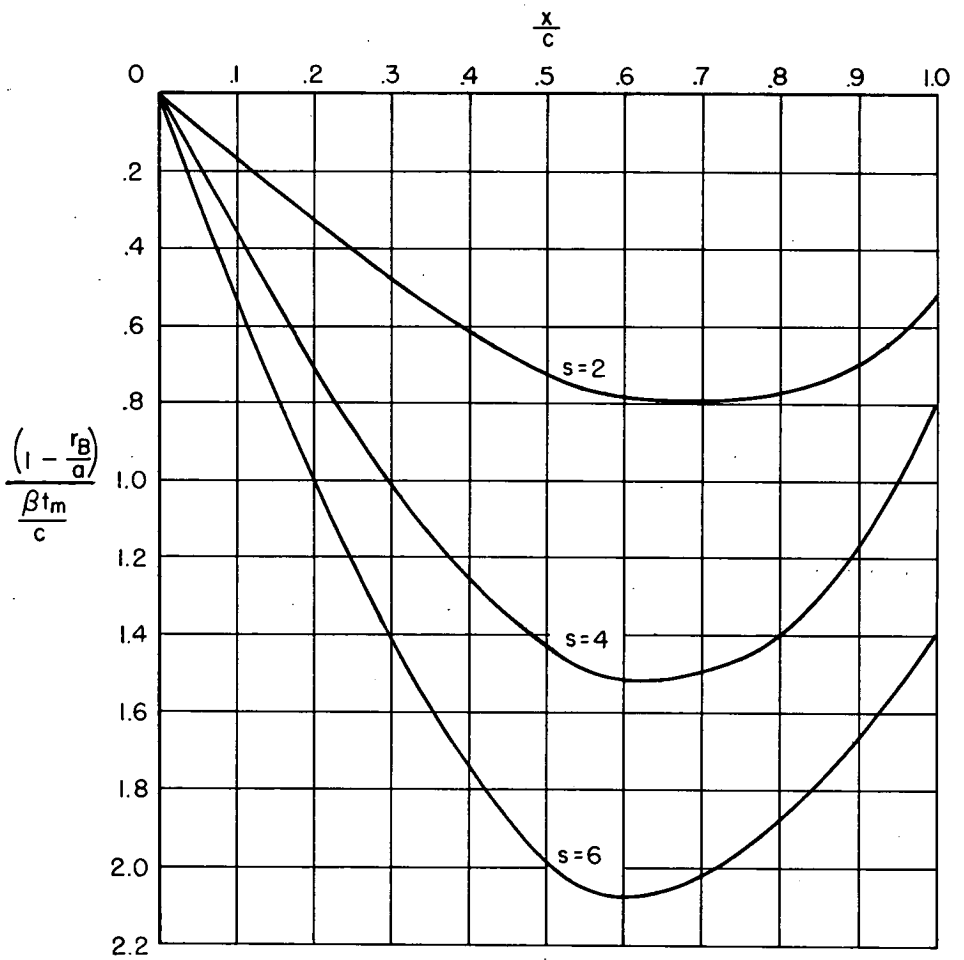

(b) $\frac{c}{\beta a} = 3$

Figure 19.- Effect of chord and span on body indentation for n = 0 harmonic.

[redacted]

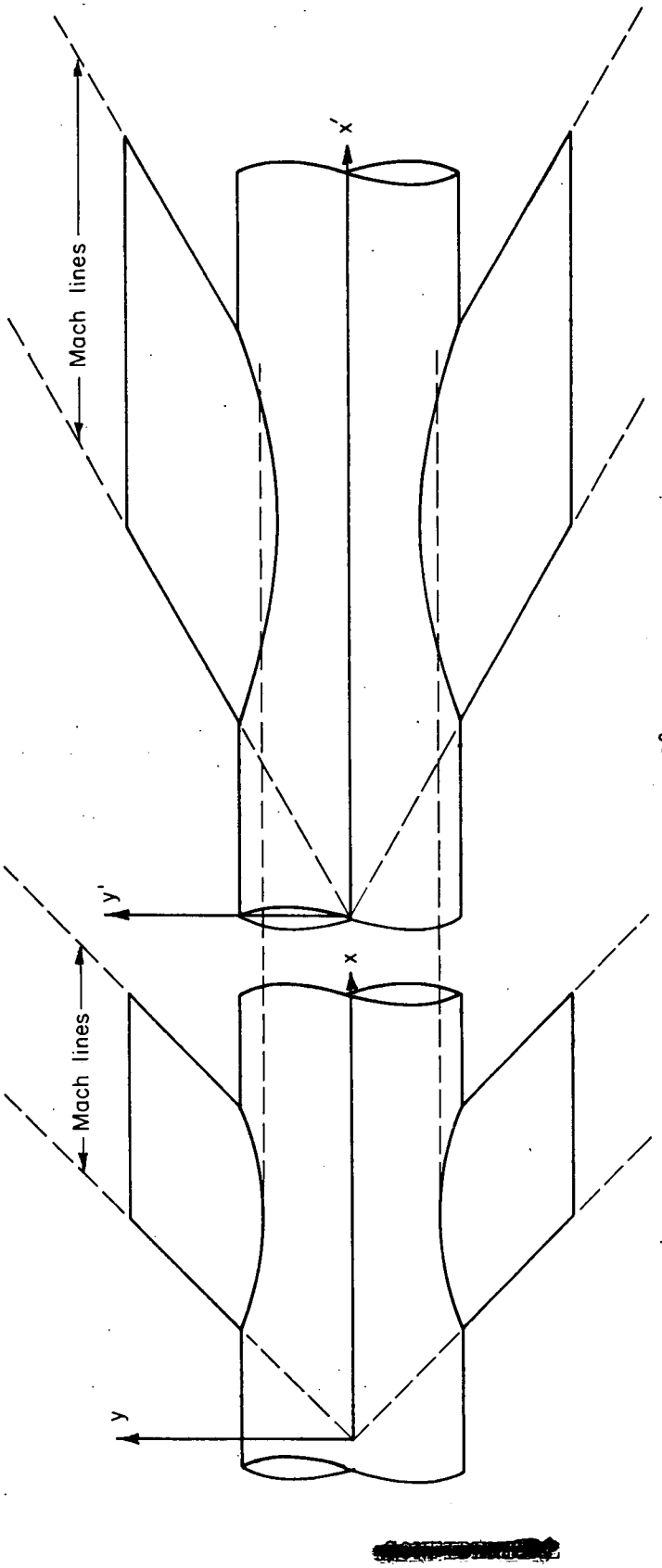

(a) $M = \sqrt{2}$ (b) M

Figure 20.- Relationship between wing-body combination and equivalent combination at $M = \sqrt{2}$.